NAVAL POSTGRADUATE SCHOOL

MONTEREY, CALIFORNIA

THESIS

DIGITAL TRACKING ARRAY FOR FM SIGNALS BASED ON OFF-THE-SHELF WIRELESS TECHNOLOGIES

by

Hui Kok Meng, Edmund

December 2007

Thesis Advisor: David C. Jenn
Second Reader: Robert D. Broadston

Approved for public release; distribution is unlimited

THIS PAGE INTENTIONALLY LEFT BLANK

REPORT DOCUMENTATION PAGE		*Form Approved OMB No. 0704-0188*

Public reporting burden for this collection of information is estimated to average 1 hour per response, including the time for reviewing instruction, searching existing data sources, gathering and maintaining the data needed, and completing and reviewing the collection of information. Send comments regarding this burden estimate or any other aspect of this collection of information, including suggestions for reducing this burden, to Washington headquarters Services, Directorate for Information Operations and Reports, 1215 Jefferson Davis Highway, Suite 1204, Arlington, VA 22202-4302, and to the Office of Management and Budget, Paperwork Reduction Project (0704-0188) Washington DC 20503.

1. AGENCY USE ONLY *(Leave blank)*	2. REPORT DATE December 2007	3. REPORT TYPE AND DATES COVERED Master's Thesis	
4. TITLE AND SUBTITLE Digital Tracking Array for Fm Signals Based on Off-The-Shelf Wireless Technologies		5. FUNDING NUMBERS	
6. AUTHOR(S) Hui Kok Meng, Edmund			
7. PERFORMING ORGANIZATION NAME(S) AND ADDRESS(ES) Naval Postgraduate School Monterey, CA 93943-5000		8. PERFORMING ORGANIZATION REPORT NUMBER	
9. SPONSORING /MONITORING AGENCY NAME(S) AND ADDRESS(ES) N/A		10. SPONSORING/MONITORING AGENCY REPORT NUMBER	

11. SUPPLEMENTARY NOTES The views expressed in this thesis are those of the author and do not reflect the official policy or position of the Department of Defense or the U.S. Government.

12a. DISTRIBUTION / AVAILABILITY STATEMENT Approved for public release, distribution is unlimited	12b. DISTRIBUTION CODE **A**

13. ABSTRACT (maximum 200 words)

The purpose of this research is to design a digital phased array for receiving and tracking a 2.4 GHz FM video signal from an unmanned air vehicle. The tracking is done using a monopulse technique. Various numbers of elements were simulated to access the pattern coverage. The beamforming and demodulation are performed digitally by a computer. Several antenna architectures were studied and the requirements for hardware components such as the analog-to-digital converters and amplifiers are specified. Several methods for generating the carrier signal for the local oscillator are also discussed. They include an independent local oscillator, a voltage controlled oscillator with feedback (i.e., a phased locked loop) and mixing with a phase shifted copy of the received signal (Bilotti's method).

14. SUBJECT TERMS Tracking,Array Antenna, Wireless Technologies,UAV, Sun and difference beams.			15. NUMBER OF PAGES 101
			16. PRICE CODE
17. SECURITY CLASSIFICATION OF REPORT Unclassified	18. SECURITY CLASSIFICATION OF THIS PAGE Unclassified	19. SECURITY CLASSIFICATION OF ABSTRACT Unclassified	20. LIMITATION OF ABSTRACT UU

Standard Form 298 (Rev. 2-89)
Prescribed by ANSI Std. 239-18

THIS PAGE INTENTIONALLY LEFT BLANK

DIGITAL TRACKING ARRAY FOR FM SIGNALS BASED ON OFF-THE-SHELF WIRELESS TECHNOLOGIES

Hui Kok Meng, Edmund
Singapore Technologies Marine Ltd.
B.E.(Electrical & Electronic Engineering), University of Glasgow, Scotland, UK, 2001

Submitted in partial fulfillment of the
requirements for the degree of

MASTER OF SCIENCE IN ELECTRICAL ENGINEERING

from the

NAVAL POSTGRADUATE SCHOOL
December 2007

Author: Hui Kok Meng Edmund

Approved by: Professor David C. Jenn
                 Thesis Advisor

                 Robert D. Broadston
                 Second Reader

                 Professor Jeffrey B. Knorr
                 Chairman, Department of Electrical and Computer Engineering

THIS PAGE INTENTIONALLY LEFT BLANK

ABSTRACT

The purpose of this research is to design a digital phased array for receiving and tracking a 2.4 GHz frequency modulation (FM) video signal from an unmanned air vehicle. The tracking is done using a monopulse technique. Various numbers of elements were simulated to access the pattern coverage. The beamforming and demodulation are performed digitally by a computer. Several antenna architectures were studied and the requirements for hardware components such as the analog-to-digital converters and amplifiers are specified. Several methods for generating the carrier signal for the local oscillator are also discussed. They include an independent local oscillator, a voltage controlled oscillator with feedback (i.e., a phased locked loop) and mixing with a phase shifted copy of the received signal (Bilotti's method).

THIS PAGE INTENTIONALLY LEFT BLANK

TABLE OF CONTENTS

LIST OF FIGURES

x

LIST OF TABLES

THIS PAGE INTENTIONALLY LEFT BLANK

EXECUTIVE SUMMARY

As a part of an ongoing project, this research aimed at designing a digital phased array for receiving and tracking a 2.4 GHz FM video signal from an unmanned air vehicle (UAV). Tracking the signal from the UAV will establish a data link for data transfer such as video, image or audio between the UAV and the ground station. The tracking is done using a monopulse technique.

An array tradeoff study was done to determine the benefits of 1 row and 2 row arrays, with 8 elements per row, in terms of the half-power beamwidths (HPBWs) of the azimuth and elevation patterns of the array. The one row array was chosen primarily due to its wide elevation pattern coverage. This eliminates the need for elevation tracking as the UAV is within the HPBW for all UAV ranges of interest. Adding a row of 8 more elements to increase the signal-to-noise ratio (SNR) will increase the cost of equipment. The additional SNR is not required, as the UAV transmitter power is sufficiently high. The sum and difference beams for the Matlab simulation of the one row array are verified with the CST Microwave Studio simulations. The printed circuit dipole element was found to have an E-plane pattern HPBW between that of an ideal dipole and a half-wave dipole.

Several approaches for the demodulation of FM signals are explored. The considerations for the choice of the approaches for the FM demodulation are the minimum circuitry requirement, the ability to conduct beamforming, the recovery of the transmitted signal and the susceptibility to phase errors and local oscillator (LO) drift. Three FM demodulation techniques are considered: Bilotti's quadrature demodulator, a local oscillator with no feedback and a digital phase locked loop (PLL) quadrature detector. All three use digital beamforming and signal processing to demodulate the FM. Simulink models of the three FM demodulation techniques show satisfactory performance for the recovery of a two-tone signal.

The simulations were done at a carrier frequency of 50 kHz instead of 2.4 GHz, to greatly save on the processing time. A LO with no feedback was chosen, as it uses the

least circuitry with satisfactory performance for the recovery of the two-tone signal. Beamforming can also be performed easily as the raw in phase (I) and quadrature (Q) data are preserved. This technique also eases the computer processing. Since no error correction needs to be computed for the LO as it does for a PLL. Simulations were also done with relative phase errors introduced in the channels and a frequency offset in the LO without feedback. The Simulink simulations indicate that the recovery of the two-tone signal can still be achieved with the expected errors.

Finally, the possible hardware components are briefly introduced and the minimum power for the receiver module was used to determine the maximum operating range of the array using the one-way Friis equation.

ACKNOWLEDGMENTS

I would like to express my gratitude to Professor David C. Jenn, who trusted me with this thesis assignment, for his patience and guidance. His valuable and sound knowledge of electromagnetism (as well as his knowledge of Matlab and its applications) gave me the encouragement and confidence to complete this thesis. His devotion, patience and sharing of information is admirable. Without the assistance of Professor Jenn, this thesis would not have been completed.

I would like to thank Robert D. Broadston, the manager of the microwave laboratory of the Naval Postgraduate School, for being my second reader, helping me set up the lab work and Matlab Simulink models. I also appreciated his sharing of his knowledge for my thesis.

I would like to thank my lovely wife Janet Gan for her support, understanding and never-ending patience with me, since I could not spend enough time with her throughout my research. I also thank my parents, Molly Poh and Franklin Hui, for supporting me all through my life in one way or another.

Lastly, I would like to thank Singapore Technologies Marine Ltd. and my boss, Tan Ching Eng, for giving me the opportunity to get my master's degree at the Naval Postgraduate School.

THIS PAGE INTENTIONALLY LEFT BLANK

I.   INTRODUCTION

A.   BACKGROUND

Phased array development began around 1958, when early radio transmitters and radars used multiple radiating elements to achieve the desired antenna radiation patterns [1]. As technologies advance, existing systems are improved and upgraded. Sometimes, new systems are created when the existing systems become obsolete. Unmanned systems and array antennas, two technologies that improve continuously, have brought many new capabilities to military operations. The superiorities of array antennas are the digital and computerized processing capabilities that can be built into them. Digital phase shifting to form a beam, the electronic and rapid beam scanning ability, and its broadband potential are the advantages of array antennas.

Since the Gulf War in the 1990s, the military has a new awareness of the importance of technological advances such as stealth ability, unmanned systems and global positioning systems (GPS) in improving the success of a war. One of these technologies is the digital phased array. It has many advantages, such as scanning rapidly without physically moving. Multiple, simultaneous beams can be achieved by the means of digital-beam forming (DBF). Error correction and self-calibration can be achieved easily in the signal processing. DBF also allows pattern control to direct the nulls in the pattern in the direction of noise jammers, and also suppresses clutter, which is a cause of degradation in range. DBF also gives the opportunity to compensate for the failure of the elements in the array. Different data rates, depending on the operating environment, can be achieved with DBF. The array antennas can be used in many applications, such as communications, data-links, radar (search and track), and electronic warfare (EW). This shows perhaps the most important advantage of these antennas: the multi-functionality.

Unmanned aerial vehicles (UAVs), one important type of unmanned system, play a very critical role in military operations. UAVs have a variety of uses, such as surveillance and reconnaissance, target recognition, battle damage assessment, EW, search and rescue, and traffic monitoring. All of these can be conducted without

endangering the life of a pilot, as they do for manned systems. Important roles for the UAVs are troop support and carrying out reconnaissance and surveillance missions, which require maintaining a data-link with troops in order to send any data collected, such as video images or audio, back to the command center.

During operations, it is imperative to continuously maintain a data and control link with the operator. This requires the ground station antenna to track the UAV so the antenna beam is pointed properly. The purpose of this research is to design and build an array to angle-track a UAV and, eventually, to accomplish the data transfer from the UAV to the ground station. The antenna type on the UAV is not a subject of this research and it will be assumed to be a low-gain omni-directional antenna. What is of concern is the array system that will be designed to achieve the purpose that was just mentioned.

Why is an array antenna selected for this application? The narrow beam of the antenna must be kept on the UAV as it moves and maneuvers. The beams of an array can track without physically moving the antenna. Digital array systems can be reconfigured and different beamwidths can be used, depending on the UAV path and the data rate desired for the type of operation. Array antenna systems can track and follow more than one UAV at a time (multiple tracking) [2]. Figure 1 shows a High Gain Advanced GPS Receiver (HAGR) phased array antenna.

Figure 1.   HAGR 16 element antenna array. From [3].

B. PHASED ARRAY TECHNOLOGY FOR MILITARY APPLICATIONS

Since 1901, array antenna technology has made tremendous progress with types that vary from linear to planar to conformal. Digital array applications enable the main beam of arrays to be steered electronically, rather than mechanically. A phased array has its radiating elements excited by the relatively phased currents and its main beam can scan the desired field continuously. Since the 1980s, phased arrays have gained wider use in radar and communication applications.

Phased array radars are used in a number of navy ships, such as the US Navy Aegis ships, the German Navy's F124 frigates and LCF frigates of the Royal Netherlands Navy [4]. The advantages of the phased array radars used in communication systems are summarized below:

1. Electronically scanning the beam and its multiple element system increases the reliability of the radar system, and maintenance is simplified by replacing the faulty elements with new ones without a need to return to the shipyard. An antenna can have a significant number of its elements destroyed and still be able to function, albeit at a reduced capability. Electronic arrays have no moving parts, do not suffer from vibration and are inherently better stabilized against ship or aircraft motion, as the electronic array simply steers the main beam counter to the detected motion.

2. It is suitable for low observable platforms as antenna elements of the array, like a microstrip patch antenna, can conform to the structure of stealthy platforms. Its agile scanning rate, with a narrow beam and lower sidelobes, gives a low probability of interception and is less vulnerable to jamming.

3. The integrated circuit (IC) technology in microwave monolithic ICs (MMICs) is being driven by the need to integrate disparate technology functions into one unit. Through the use of IC technology, phased arrays can reach improved cost, size, and weight metrics that have previously prevented the widespread adoption in mass market scenarios. The high power handling capability and low loss of ferrite phase shifters allow power amplifiers, low

noise amplifiers and phase shifters to be chosen to achieve high processing performance, with relatively little impact to cost. Hence the solid state and IC technologies will benefit the phased array in terms of costs, weight and reliability [5, 6].

4. Its ability to create multifunction systems (radar, sensing, communications, etc.) with a single device enabled by the system's software-driven nature increases the tactical flexibility of its operational employment. This capability is explained in the following scenarios:

- The radiated power from each element can be adjusted when each element has its own transmitter. At the expense of cost, the controlling of the radiated power in sectors addresses the concern for emission control and co-site interference.

- The elements can be programmed to communicate with multiple UAVs by scanning one single beam rapidly or producing multiple, independent beams. This would increase the dwell time on each UAV.

- The multifunction system reduces the number of antennas on the military platforms, hence reducing weight and the radar cross section of the platform.

- Its flexibility in electronic control allows for customized software solutions to address different user scenarios with one platform [5].

- A graceful degradation is allowed when some of the elements are damaged enabling the array system to continue functioning.

The frequency bandwidth is a major design challenge for the array system as bandwidth is a scarce commodity in modern communications systems, with the Federal Communications Commission (FCC) deciding which parts of the spectrum can be used for emerging communication standards. Despite the multi-functionality of the current arrays, different functions need different bands, due to the unique characteristics and behaviors of the electromagnetic waves in different frequency bands. Multifunction

arrays can be used for surveillance, tracking, communications, direction finding and weapon guidance purposes. The radar should be designed in lower bands for longer range. The AN/SPY-1D operates in S band. Current electronic support equipment operates within the range from 2 to 20 GHz. However, due to the dense electronic environment, it is very difficult for the electronic warfare operators to detect radars operating in the UHF band in the littoral waters.

The complexity of the phased arrays will increase the cost. Commercial off-the-shelf (COTS) hardware is to be exploited to reduce the cost of the phased arrays. The ultimate aim of the antenna engineer is to decrease the cost of the phased array antennas without sacrificing performance [2].

C.   PREVIOUS WORK

This research is part of the ongoing project that started with the thesis by Bartee [7]. Esswein [8] and Gezer [2] continued the work and demonstrated the feasibility of building a digital phased array with available COTS hardware.

Bartee designed and constructed the distributed phased array at X-band.

Esswein constructed a 24-element, three-dimensional, dual-ground plane, active phased array. A Genetic Algorithm (GA) was used to determine the element excitations and the measured radiation beam was in agreement with the theoretical calculations. The modulator feeding each printed antenna element used for this array was the Analog Devices AD8346EVAL quadrature modulator board, which is now being incorporated into a transmit/receive (T/R) module for radar applications.

Gezer constructed a 1 by 8 phased array to track a signal transmitted continuously by a UAV operating at 2.4 GHz. This array used a monopulse difference beam to track the UAV signal. The array was designed based on typical UAV operational requirements, which led to the selection of the array parameters, such as the number of elements and spacing.

D.   SCOPE OF RESEARCH

State of the art technology in electronic systems is a means to increase the information superiority and provide the decision makers with a well described tactical picture of the war scene. UAVs can carry out many reconnaissance and surveillance missions. They also provide the necessary information to the troops by being integrated into the network-centric warfare elements as seen in Figure 2.
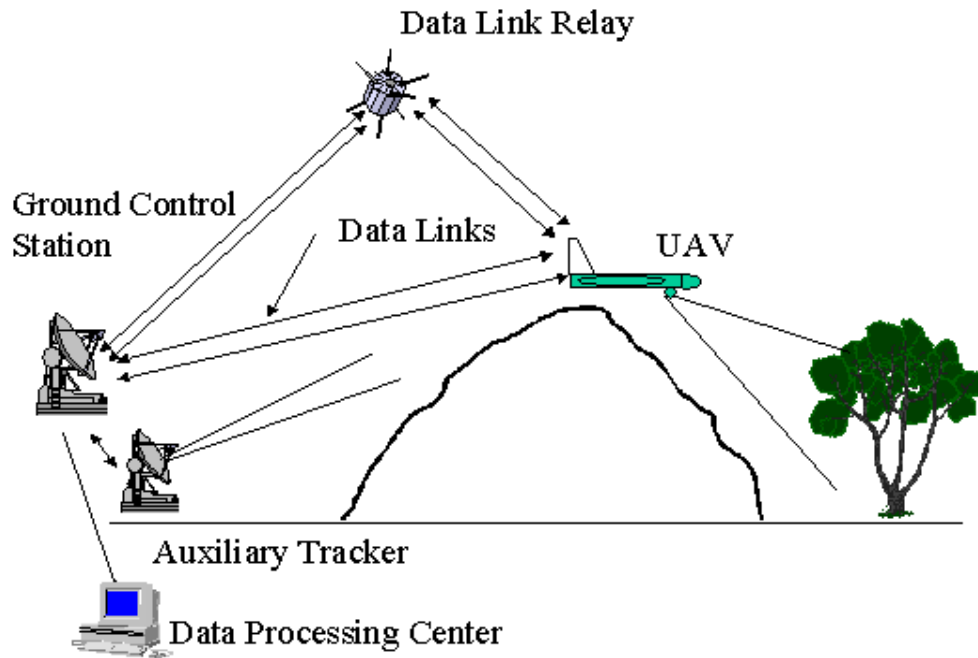
Figure 2.   The cooperation among the elements of a UAV system. From [10].

As an element of the network, the ground control stations of UAV systems can exploit the phased array technology. Array antennas are a very sophisticated means to accomplish accurate UAV tracking and maintain a good data-link.

The research goal was to design a digital phased array for tracking and receiving FM video signals transmitted at 2.4 GHz from a UAV. The design incorporates COTS hardware to reduce cost. Simulation is another way to reduce the cost of the design and comprehend the consequences of design changes before manufacturing, and to see if there needs to be any adjustment. Thus, the design of the tracking array antenna system is verified through simulations before being constructed [2].

E.   ORGANIZATION OF THESIS

Chapter II discusses the concepts of arrays. The concepts of a digital antenna and digital beamforming are explained, and the mathematical theory for arrays with ground planes is elaborated. Amplitude comparison monopulse systems, and how tracking of the UAV is achieved, along with external causes of errors, are mentioned.

Chapter III addresses the results and analysis of the array tradeoff study. It discusses the results obtained for the 1 row and 2 row arrays with 8 elements. Also, the effect of polarization is studied.

Chapter IV addresses the FM demodulation techniques being considered. Several methods for generating the carrier signal are also discussed. They include an independent local oscillator, a voltage controlled oscillator with feedback (i.e., a phased locked loop) and mixing with a phase shifted copy of the received signal (Bilotti's method).

Chapter V discusses the system architecture of the array and its considerations. Hardware implementation using COTS components is also described.

Chapter VI summarizes what was done in this research and gives recommendations for future work.

THIS PAGE INTENTIONALLY LEFT BLANK

II.   TRACKING ARRAY DESIGN

A.   WHY AN ARRAY ANTENNA?

An antenna array is a configuration of individual radiating elements that are arranged in space to produce a directional radiation pattern. Single-element antennas have broad and low directivity radiation patterns, which are not suitable for long distance communication or accurate tracking. High directivity can be achieved by increasing the electrical dimensions of the single-element antennas in terms of wavelength, hence its physical size. This makes the antenna too cumbersome for mobile operations. The alternative is to combine multiple electrically small antennas to form an array. Antenna arrays come in various geometrical configurations, including linear, planar and volumetric. The planar antenna array is often used in communication and radar applications, and therefore this general configuration will be analyzed [11].

Conventional phased arrays employ microwave circuits to distribute signals to the elements or, on receive, collect signals from the elements. These beamforming networks (or beamformers), as shown in Figure 3, can be bulky, narrowband and lossy. Some of these problems can be avoided by using digital beamforming.
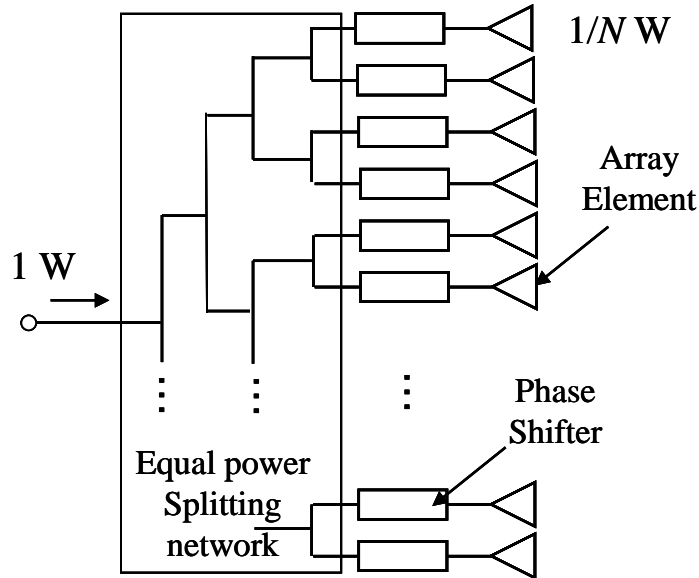
Figure 3.   Conventional microwave beamforming network. From [12].

9

B.   DIGITAL ARRAYS[1]

The basic architecture of a digital array is shown in Figure 4. For a two-way communication application, each element must be capable of transmission and reception. In the transmit channel, the waveform is generated and amplified before passing to the array element. On receive, the signal is amplified and detected. The detected signals are collected by a processor which forms the beam and performs other communication functions.

In order for all of the elements to send and collect data coherently, a common frequency (phase) reference must be distributed to all of the elements. This signal is referred to as the local oscillator (LO) signal. The elements must also be time synchronized so that transmission can occur simultaneously and the transmitted signals arrive at the other end of the link at the same time.
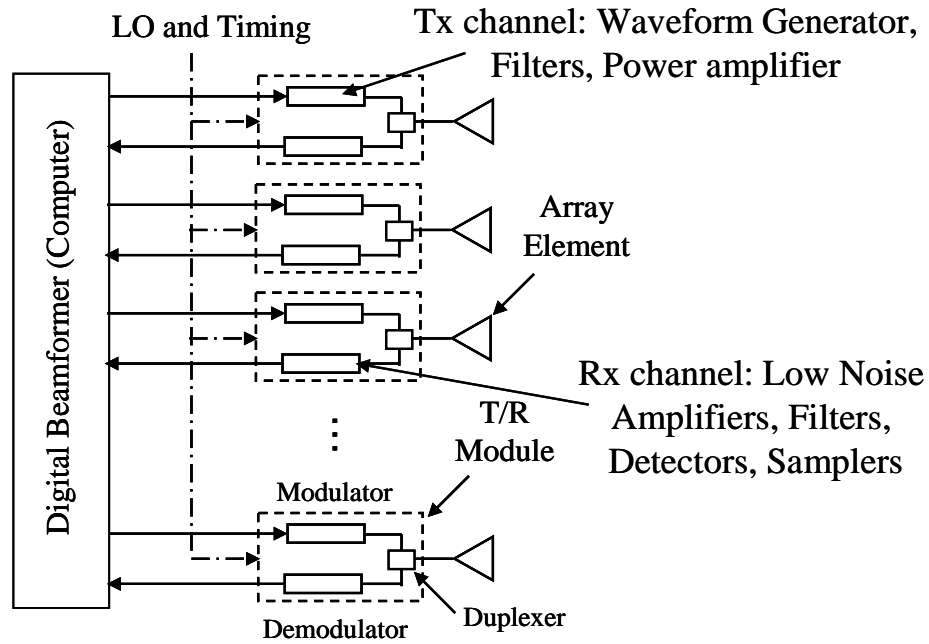
Figure 4.   Generic digital antenna architecture From [12].

Generally the array has a modular architecture where the transmit (Tx) and receive (Rx) functions are channeled. The transmit portion generates the waveform,

---

[1] Much of the material in this section is adapted from unpublished notes by Prof. D. Jenn.

amplifies and filters it before passing it to the antenna. In modern arrays, the waveform is generated using a direct digital synthesizer (DDS). In its simplest form, a DDS is a clock and memory with a stored waveform. The waveform is read out at a rate determined by the clock. The DDS output is usually a baseband signal that has to be upconverted, although recent DDS clock speeds are achieving 2 GHz. Therefore, at VHF radar frequencies and below, it may be possible to amplify the DDS output directly without upconversion. For the tracking application, this research is concerned only with the receive function. Therefore, the remaining discussion only addresses the receive channel.

On the receive side the returned signal is amplified with a low noise amplifier (LNA), downconverted, filtered and then sampled. State of the art analog-to-digital converters (ADCs) are in the 2 GHz range, so at VHF and below it may be possible to sample the waveform directly without downconverting.

The in-phase (I) and quadrature (Q) form of the data are handled by the hardware. If the signal at carrier frequency $\omega_c = 2\pi f_c$ is:

$$s(t) = A(t)\cos\left[2\pi f_c t + \Phi(t)\right] \tag{1}$$

the in-phase and quadrature representation is:

$$s(t) = I(t)\cos(2\pi f_c t) - Q(t)\sin(2\pi f_c t) \tag{2}$$

where

$$\begin{aligned} I(t) &= A(t)\cos\left[\Phi(t)\right] \\ Q(t) &= A(t)\sin\left[\Phi(t)\right] \end{aligned} \tag{3}$$

and

$$\begin{aligned} A(t) &= \sqrt{I(t)^2 + Q(t)^2} \\ \Phi(t) &= \tan^{-1}\left[\frac{Q(t)}{I(t)}\right] \end{aligned} \tag{4}$$

The signal is conveniently shown in the I/Q plane (Figure 5), where the distance from the origin is $A(t)$ and the rotation from the I axis is $\Phi(t)$.

11

Figure 5 also shows a quadrature demodulator, the Analog Devices AD8347 [14], which operates from 800 MHz to 2.6 GHz with a 60 MHz instantaneous bandwidth. The demodulator has differential outputs (I^+, I^-, Q^+, and Q^-) for obtaining the baseband in-phase and quadrature components of the received signal. The components are given by:

$$I = I^+ - I^-$$
$$Q = Q^+ - Q^-$$

(5)

The hardware aspects are discussed further in Chapter V, Section A.
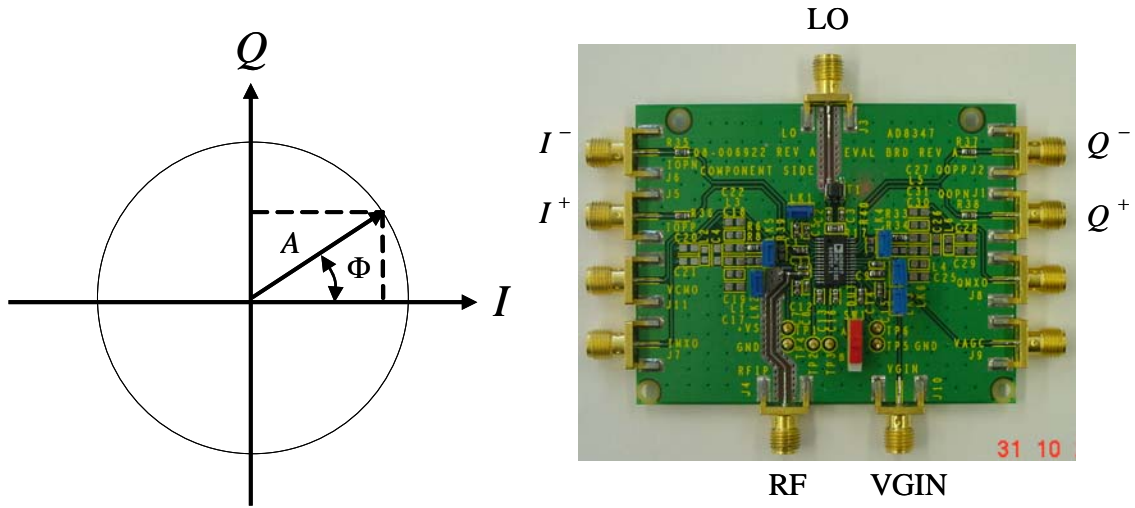
Figure 5.   *I/Q* signal diagram (left) and the AD8347 quadrature demodulator (right). From [12].

The demodulation process is analyzed using the complex envelop of the signal $u(t)$ [15]:

$$u(t) = I(t) + jQ(t)$$
$$s(t) = \text{Re}\left\{u(t)e^{j\omega_c t}\right\}$$
$$= \frac{1}{2}\left[u(t)e^{j\omega_c t} + u*(t)e^{-j\omega_c t}\right].$$

(6)

The mixing process (shown in Figure 6) is equivalent to multiplying the received signal with

$$\cos \omega_{LO} = \frac{1}{2}\left(e^{j\omega_{LO}t} + e^{-j\omega_{LO}t}\right) \tag{7}$$

in the *I* channel and with

$$-\sin \omega_{LO} = -\frac{1}{2j}\left(e^{j\omega_{LO}t} - e^{-j\omega_{LO}t}\right) \tag{8}$$

in the *Q* channel.
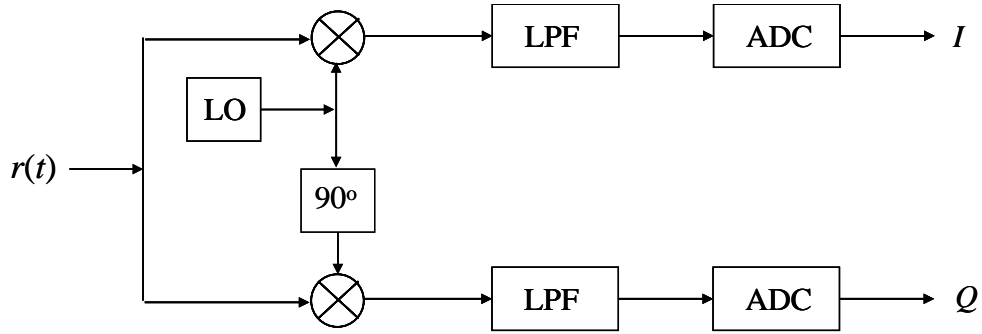
Figure 6.   Quadrature demodulation process. From [12].

For the in-phase channel:

$$
\begin{aligned}
r(t)\cos \omega_{LO} &= \frac{1}{4}\left[u(t)e^{j\omega_c t} + u*(t)e^{-j\omega_c t}\right]\left(e^{j\omega_{LO}t} + e^{-j\omega_{LO}t}\right) \\
&= \frac{u(t)}{4}e^{j(\omega_c+\omega_{LO})t} + \frac{u(t)}{4}e^{j(\omega_c-\omega_{LO})t} \\
&\quad + \frac{u*(t)}{4}e^{-j(\omega_c-\omega_{LO})t} + \frac{u*(t)}{4}e^{-j(\omega_c+\omega_{LO})t} \\
&= \mathrm{Re}\left\{\frac{u(t)}{2}e^{j(\omega_c+\omega_{LO})t}\right\} + \mathrm{Re}\left\{\frac{u(t)}{2}e^{j(\omega_c-\omega_{LO})t}\right\}
\end{aligned}
\tag{9}
$$

where $\mathrm{Re}\{.\}$ is the real operator and the $*$ is complex conjugate.

If direct down conversion is used (no intermediate frequency, $\omega_{LO} = \omega_c$), then the first term is at frequency $2\omega_c$, which is filtered by the low pass filter (LPF). The second term is the desired base band signal.

13

A similar analysis for the quadrature channel gives two terms:

$$-r(t)\sin\omega_{LO} = \text{Im}\left\{\frac{u(t)}{2}e^{j(\omega_c - \omega_{LO})t}\right\} - \text{Im}\left\{\frac{u(t)}{2}e^{j(\omega_c + \omega_{LO})t}\right\}. \tag{10}$$

where $\text{Im}\{.\}$ is the imaginary operator and, similar to the I channel, the second term is at frequency $2\omega_c$ and is filtered. The I and Q outputs are combined in the processor to form the complex signal [12].

C.   DIGITAL BEAMFORMING

For a simple linear array along the z axis in Figure 7, the array factor is given by:

$$AF(\theta,\phi) = \sum_{n=1}^{N} w_n \exp\left[j\beta d_n \cos\theta\right] = \sum_{n=1}^{N} A_n e^{j\alpha_n} \exp\left[j\beta d_n \cos\theta\right] \tag{11}$$
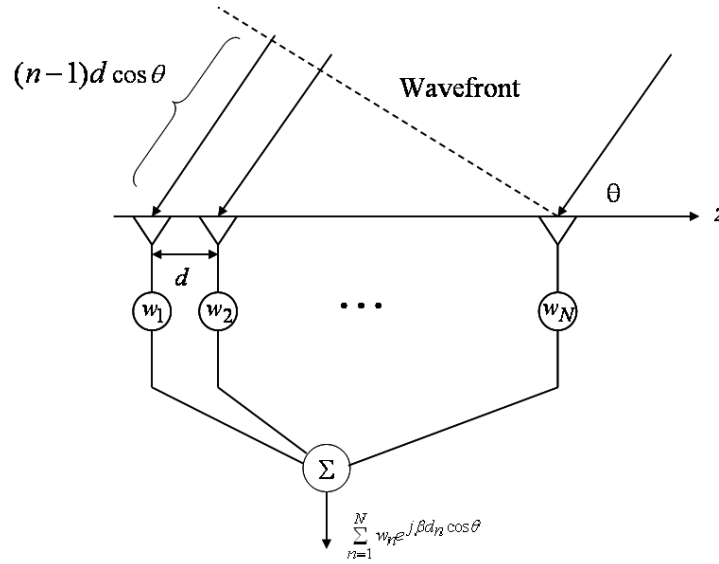
Figure 7.   Digital array beamforming on receive. From [12].

where N is the number of elements, $\beta = 2\pi/\lambda$ (λ is wavelength), $w_n = A_n e^{j\alpha_n}$ is a complex weight added by the processor and

$$d_n = \frac{[2n - (N+1)]}{2}d \tag{12}$$

is the location of element n relative to the origin at the center of the array.

14

The demodulators provide spatial samples of the exponential factor in Equation (11):

$$I_n = \cos\left[j\beta d_n \cos\theta\right] \tag{13}$$

$$Q_n = \sin\left[j\beta d_n \cos\theta\right] \tag{14}$$

Therefore, to obtain a response equivalent to a beam scanned in the direction θ_s the weights must be given by:

$$w_n = \exp\left[-j\beta d_n \cos\theta_s\right] \tag{15}$$

Note that compensation for any phase errors in the hardware could be included in the exponent of w_n. They can be obtained by calibration [12].

D.   ARRAYS WITH GROUND PLANES

This section derives the formulas used in the Matlab codes to obtain the radiation pattern of a two-dimensional array with a rectangular element lattice.[2] Figure 8 shows a planar array of point sources in the x-z plane.
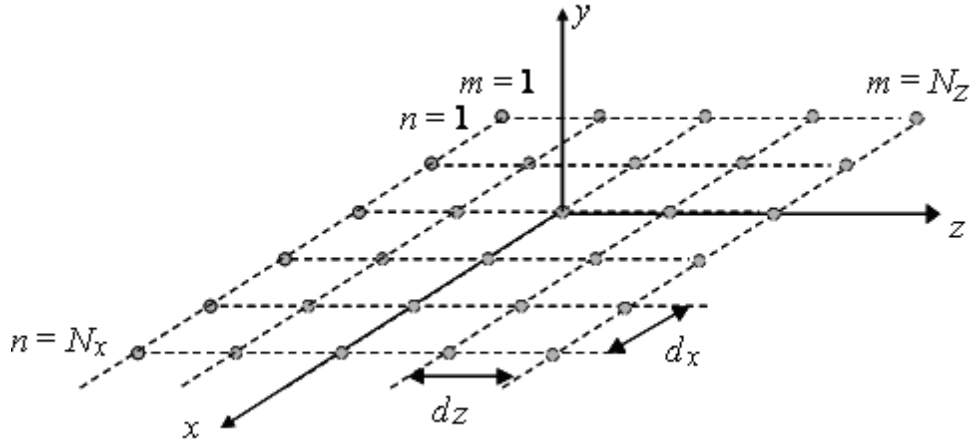
Figure 8.   Planar array centered at the origin. After [16].

---

[2] This analysis is updated from unpublished notes by Prof. David C. Jenn of NPS.

The pattern angles θ and ϕ and the array orientation are shown in Figure 9.
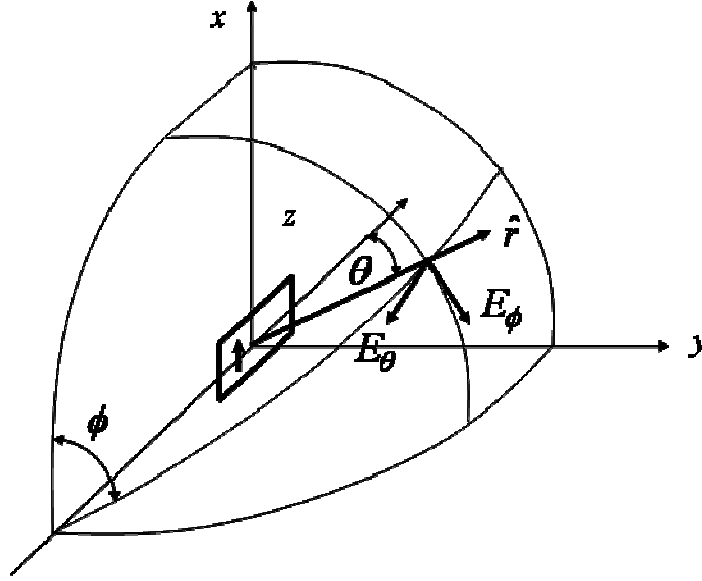
Figure 9.   Array orientation and pattern angles θ and ϕ. After [17].

If the array is centered at the origin, then the element locations can be written as:

$$
\begin{aligned}
x_n &= \frac{2n-(N_x+1)}{2}d_x, \quad n=1,...,N_x \\
z_m &= \frac{2m-(N_z+1)}{2}d_z, \quad m=1,...,N_z
\end{aligned}
\tag{16}
$$

where d_x and d_z are the lattice dimensions and N_x and N_z are the number of elements along x and z, respectively. The array factor is:

$$
AF = \sum_{n=1}^{N_x}\sum_{m=1}^{N_z} A_{mn} e^{j\beta x_n \sin\theta \cos\phi} e^{j\beta z_m \cos\theta}
\tag{17}
$$

If the feeding arrangement results in a separable distribution (which is common) then $A_{mn} = A_m A_n$ and

$$
AF = AF_x AF_z = \sum_{n=1}^{N_x} A_n e^{j\beta x_n \sin\theta \cos\phi} \sum_{m=1}^{N_z} A_m e^{j\beta z_m \cos\theta}
\tag{18}
$$

16

Furthermore, if phases are introduced to scan the beam to the direction (θ_s, ϕ_s) then

$$AF = \sum_{n=1}^{N_x} A_n e^{j\beta x_n(\sin\theta\cos\phi - \sin\theta_s\cos\phi_s)} \sum_{m=1}^{N_z} A_m e^{j\beta z_m(\cos\theta - \cos\theta_s)} \tag{19}$$

Finally, if the array is uniformly excited ($A_{mn} = 1$), the sum becomes a geometric series with the following closed form result [18]:

$$AF = AF_x AF_z = \frac{\sin(N_x\psi_x/2)}{\sin(\psi_x/2)} \frac{\sin(N_z\psi_z/2)}{\sin(\psi_z/2)} \tag{20}$$

where

$$\psi_x = \beta d_x(\sin\theta\cos\phi - \sin\theta_s\cos\phi_s)$$
$$\psi_z = \beta d_z(\cos\theta - \cos\theta_s)$$

Now, if the array is placed at height h above a perfect electric ground plane of infinite extent, then the method of images can be used to compute the field above the ground plane. The total array (sources plus images) can be considered as a two-element array along the y axis, where each element itself is a planar array as shown in Figure 10.
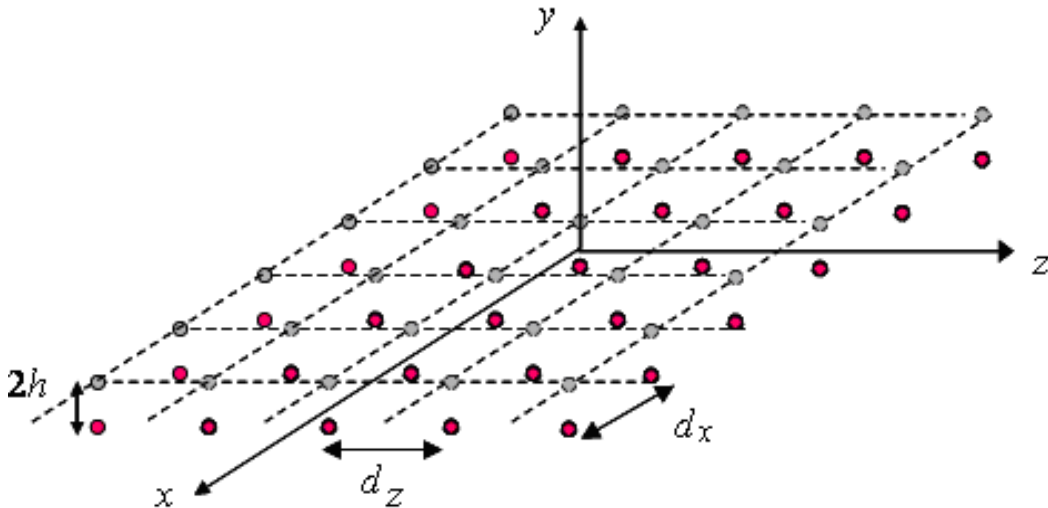
Figure 10.   Two element linear array along the y axis, where each element is a planar array. After [16].

17

The ground plane factor (*GF*) for a two-element linear array along the *y* axis, with the images out of phase with the sources is:

$$GF = e^{j\beta h \sin\theta \sin\phi} - e^{-j\beta h \sin\theta \sin\phi} = 2j\sin(\beta h \sin\theta \sin\phi) \tag{21}$$

The total normalized pattern factor is obtained using the principle of pattern multiplication

$$\begin{aligned}
F(\theta,\phi) &= (AF_x \cdot AF_z)_{\text{norm}} \cdot GF_{\text{norm}} \cdot EF_{\text{norm}} \\
&= (AF_x \cdot AF_z \cdot GF \cdot EF)_{\text{norm}} \\
&= \frac{\sin(N_x\psi_x/2)}{N_x\sin(\psi_x/2)} \frac{\sin(N_z\psi_z/2)}{N_z\sin(\psi_z/2)} \sin(\beta h \sin\theta \sin\phi) EF_{\text{norm}}
\end{aligned} \tag{22}$$

where EF_{norm} is the normalized element factor.

In general, the element factor will have both θ and ϕ components, and therefore *F* has both components as well. Referring to Figure 9, the dipoles are aligned with the *x* axis (vertical polarization). For a half-wave dipole along the *x* axis, the element factors are (see Appendix A):

$$\begin{aligned}
EF_\theta &= \frac{j\eta_o I_m\, e^{-j\beta r}}{2\pi r}\left[\frac{\cos\left(\frac{\pi}{2}\sin\theta\cos\phi\right)}{1-\sin^2\theta\cos^2\phi}\right]\cos\theta\cos\phi \\
EF_\phi &= -\frac{j\eta_o I_m\, e^{-j\beta r}}{2\pi r}\left[\frac{\cos\left(\frac{\pi}{2}\sin\theta\cos\phi\right)}{1-\sin^2\theta\cos^2\phi}\right]\sin\phi
\end{aligned} \tag{23}$$

To normalize these equations the leading factor $\dfrac{j\eta_o I_m\, e^{-j\beta r}}{2\pi r}$ is simply removed.

If the dipoles are ideal (with constant current and length, $l \ll \text{l}$), instead of half wave dipoles then the terms in square brackets [ ] are reduced to 1 and *l* is added to the leading factor. Therefore, after normalization of the element factors, only the trigonometric functions to the right of the bracketed terms remain [14]. This concept is used in the Matlab codes as shown in Appendix B.

18

E.   AMPLITUDE COMPARISON MONOPULSE SYSTEM

The tracking technique for the UAV application is an amplitude comparison monopulse system [2]. Amplitude monopulse direction finding is a common technique employed in radar systems to improve the accuracy with which the direction of the arrival of a single pulse can be estimated. Two "squinted" beams are formed simultaneously, such that they overlap at the 3 dB points of the beams, as shown in Figure 11.
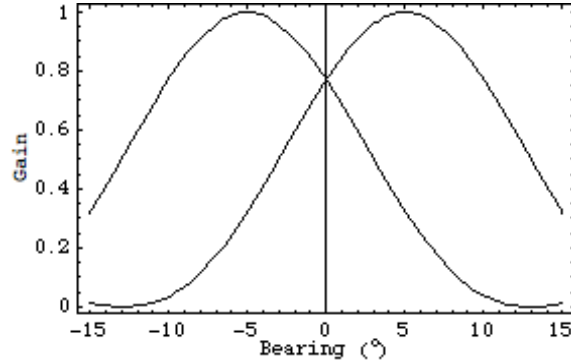
Figure 11.   Two overlapping beams. From [20].

By comparing the relative amplitude of the voltages of the signal being tracked out of the two beams, its position in the beams can be determined with an accuracy dependent on the signal-to-noise ratio (SNR). A common rule of thumb is that the accuracy of a tenth of beamwidth can be achieved with an SNR of 10 dB [18]. The difference of the amplitudes obtained from these two beams (the difference beam) gives the angular error. If the phase of the sum pattern is compared to that of the difference pattern, the direction of the angular error is found, as illustrated in Figure 12.
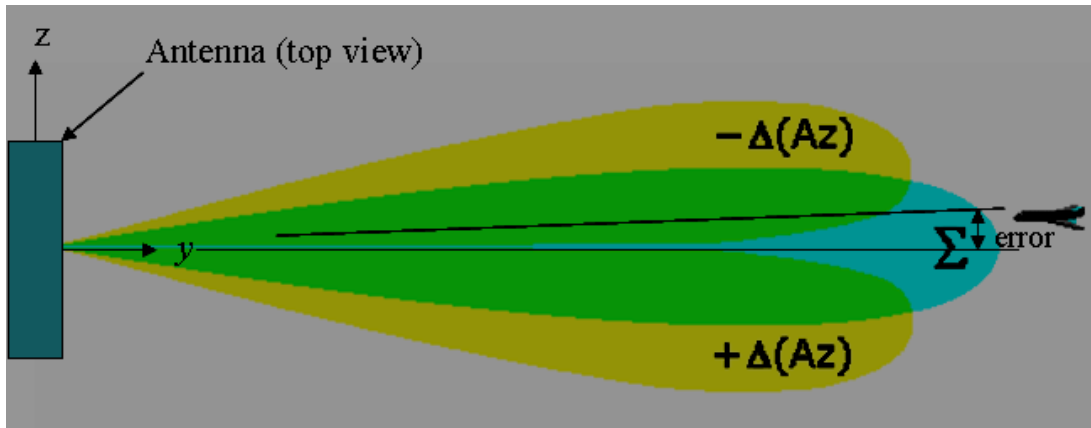
Figure 12.   Illustration of azimuth sum and difference beams. After [20].

19

The sum beam is used for transmission and the difference and sum beams are used together for the receive side in monopulse systems. The sum and difference beams are also shown in Figure 13.
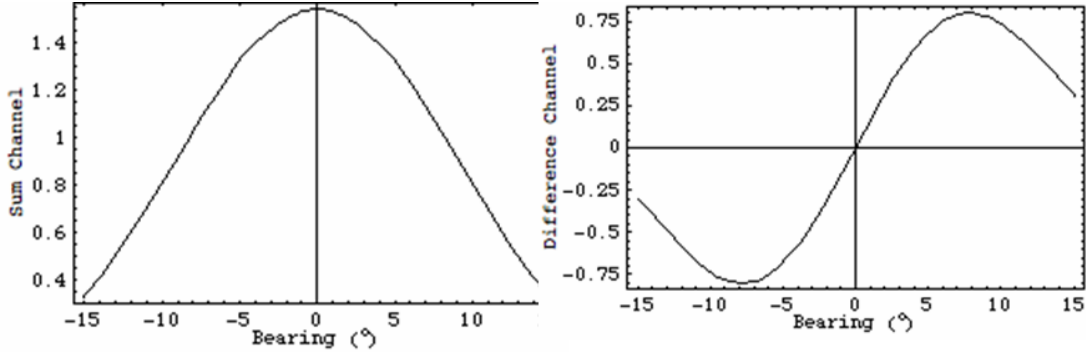
Figure 13.   Sum and difference beam output voltages. From [20].

The ratio of the difference beam to the sum beam is used to generate the angle error difference. The tracking process uses the complex voltage ratio:

$$\frac{\Delta}{\Sigma} = \frac{\text{difference voltage}}{\text{sum voltage}} \tag{24}$$

The complex voltage in Equation (25) can be separated into the real and imaginary terms:

$$\text{Re}\left\{\frac{\Delta}{\Sigma}\right\} = \frac{|\Delta|}{|\Sigma|}\cos\delta \tag{25}$$

$$\text{Im}\left\{\frac{\Delta}{\Sigma}\right\} = \frac{|\Delta|}{|\Sigma|}\sin\delta \tag{26}$$

where δ is the relative phase between sum and difference channels. Only the $\text{Re}\left\{\frac{\Delta}{\Sigma}\right\}$ is processed, as it defines the side of the null with the sign of the ratio and the signal information exists only in the real term of the ratio [17].

The plot of the pattern angle versus normalized difference to sum voltage ratio is shown in Figure 14.
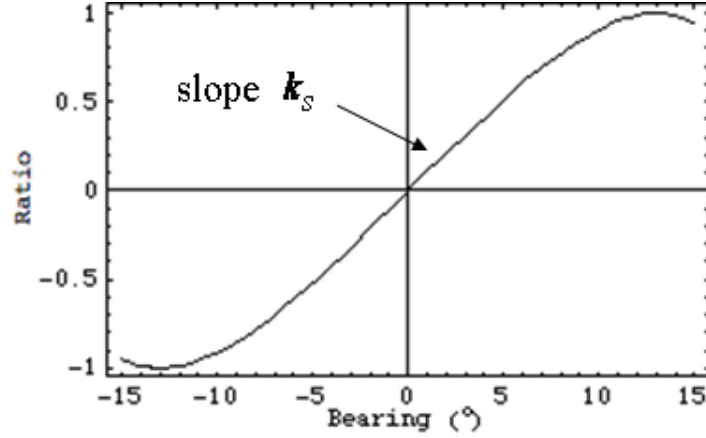
Figure 14.   Normalized difference to sum voltage ratio versus the pattern angle. From [20].

The slope in the linear region creates an error signal that helps the difference null to correct the beam, such that the target signal is within the null. This ratio is proportional to the multiplication of the slope constant k_s with the pattern angle in degrees as:

$$\frac{\Delta}{\Sigma} \approx k_s \theta, \ |\theta| \leq \frac{\theta_B}{4} \tag{27}$$

where θ_B is the half-power beamwidth (HPBW). The principle mentioned above is exploited in the tracking system of this array application. It must also be noted that the accuracy of this techniques can be affected by unwanted multipath reflections [2].

F   OTHER EXTERNAL CAUSES OF ERROR

1.   Multipath

This phenomenon occurs when a signal is reflected from the external environment, such as the terrain and other objects. The signal reaches the receiver from different paths and enters the antenna from different points on its main beam or sidelobes. The elevation tracking errors are contributed to by smooth highly reflecting ground

surfaces. Diffuse scattering from buildings or rough surfaces cause both azimuth and elevation tracking errors. The multipath errors increase as the altitude of the target gets lower.

A rms value of the multipath error is calculated from [21]:

$$\sigma_E = \frac{\rho \theta_B}{\sqrt{8 G_{se}(peak)}} \tag{28}$$

where ρ is the magnitude of the surface reflection coefficient, θ_B is antenna half-power beamwidth (HPBW) and $G_{se}(peak)$ is the power ratio of the tracking antenna sum-pattern peak to the error-pattern peak sidelobe level at the angle of arrival of the image signal. One of the objectives in looking at a planar array is to reduce the effect of multipath. Adding more rows decreases the elevation HPBW (θ_B) and also decreases σ_E according to Equation (29).

2.   Crosstalk Caused by Cross-Polarized Energy

Crosstalk, or cross-polarization coupling, is due to the cross-polarized energy of the source, like the undesired capacitive, inductive or conductive coupling from one circuit, part of a circuit or channel to another. This effect is generally negligible with a good array antenna element design. However, in situations where crosstalk is significant, a large tracking error will result in the loss of track.

3.   Troposphere Propagation

In the troposphere, which includes altitudes between 0 through 10 km of the surface, the variation of the air density, dielectric constants and the thickness of the clouds causes beam bending. Tropospheric refraction can lead to a difference in the sensed direction from the bent ray and the actual direction. At standard atmosphere conditions and short range, this error is not significant [2].

G.   SUMMARY

Normally in a digital array, each element can act as a transmitter and receiver. A LO is used to synchronize the elements to enable concurrent transmission and reception of signals. The digital beamforming concept is discussed. The ground plane effect on the radiation pattern due to the image created by the ground plane is derived. The tracking technique used is an amplitude comparison monopulse system where the sum and difference beams help in accurately tracking the UAV. In the next chapter, the computed array patterns are compared to simulated pattern using CST Microwave Studio.

THIS PAGE INTENTIONALLY LEFT BLANK

III. ARRAY TRADEOFF STUDY

This chapter addresses the antenna requirements for the array design. The antenna requirements are the scan range, HPBW and coverage in elevation based on the UAV range and altitude.

A.   HALF-POWER BEAMWIDTHS

Several array antenna analyses were done to determine the suitable array configuration for the tracking function. Gezer [2] designed and built a linear array of 8 elements. The question was whether increasing the number of elements to form a planar array would improve the tracking and range performance. First, a 2 by 8 element array is compared to the original 1 by 8 element array to determine the worthiness of using a larger number of elements. Next, the difference and sum beam patterns are compared with the results generated using the CST Microwave Studio simulations from the thesis by Gezer.

Simulations used the following parameters: $N_x = 1$ or 2, $N_z = 8$, $d_x = 10$ cm, $d_z = 6.5$ cm, $h = 0.25\lambda$. The azimuth and elevation patterns were computed for 2.4 GHz using the Matlab codes in Appendix B. Figure 15 shows the elevation patterns of arrays with 1 and 2 rows ($N_x = 1$, 2). The half-power angles are indicated by the arrows with the degrees shown. From Figure 15, the half-power beamwidth of a 1 row array is $80°$ and the HPBW of a 2 row array is $34°$. An ideal dipole is used as the array element.
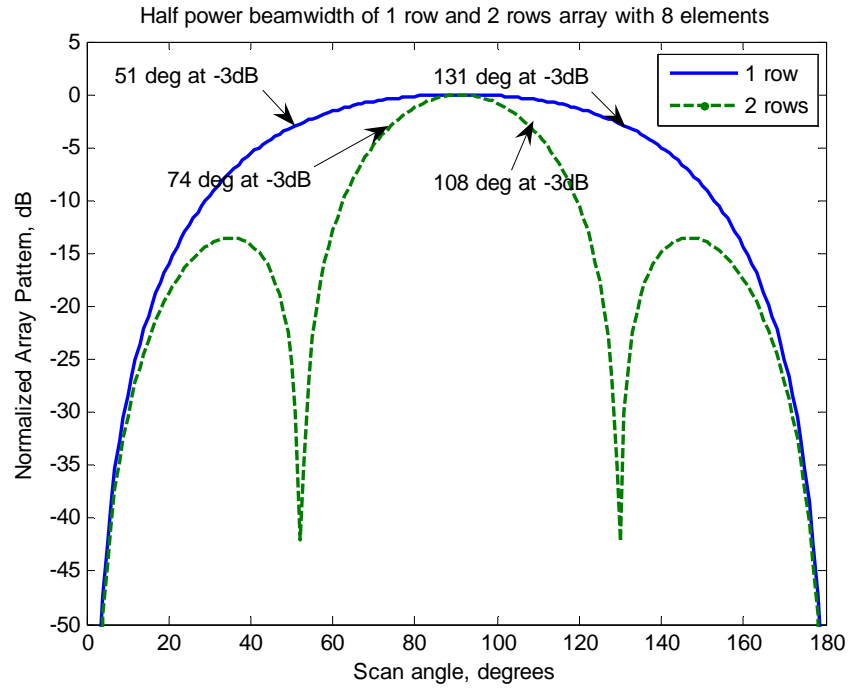
Figure 15.　Elevation plane HPBW comparison.

In order to have the largest values of gain in the coverage region, the array can be tilted back such that its HPBW point touches the horizon, as shown in Figure 16. The range of elevation angles, as the UAV flies at an altitude of 300 m, is shown in Figure 17.
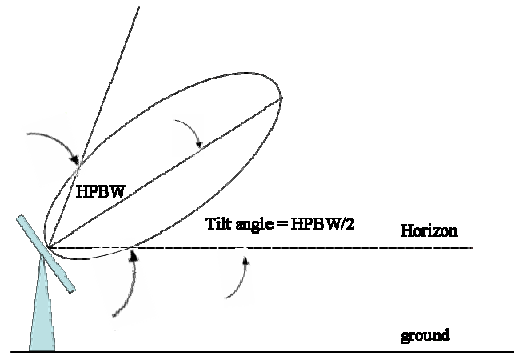
Figure 16.　Tilting of array for maximum elevation coverage.
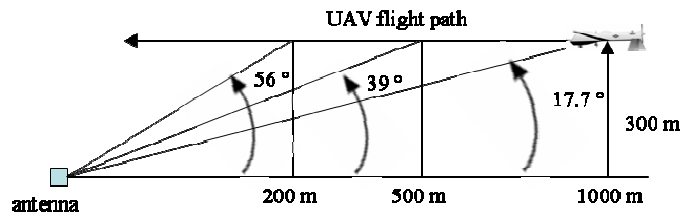
Figure 17.　Elevation angles at various ranges.

26

The UAV is within the HPBW of a one row array for all the angles shown in Figure 17. For the 2 row array, the UAV is in the HPBW at ranges greater than 560 m. Therefore, elevation tracking would have to be done at close ranges. One advantage of the 2 row array is that a null is pointed at the ground. The null and the low sidelobe help to suppress multipath.

The same Matlab code in Appendix B is used to generate the azimuth pattern of the array antenna for three different conditions, which are shown in Figure 18. The three conditions are as follows:

1. 1 row array at θ_s =90° and ϕ_s =90°,

2. 2 row array at θ_s =90° and ϕ_s =90°, and

3. 1 row array at θ_s =40° and ϕ_s =90°.

It is noticed that the azimuth pattern is the same for the first and second configurations.
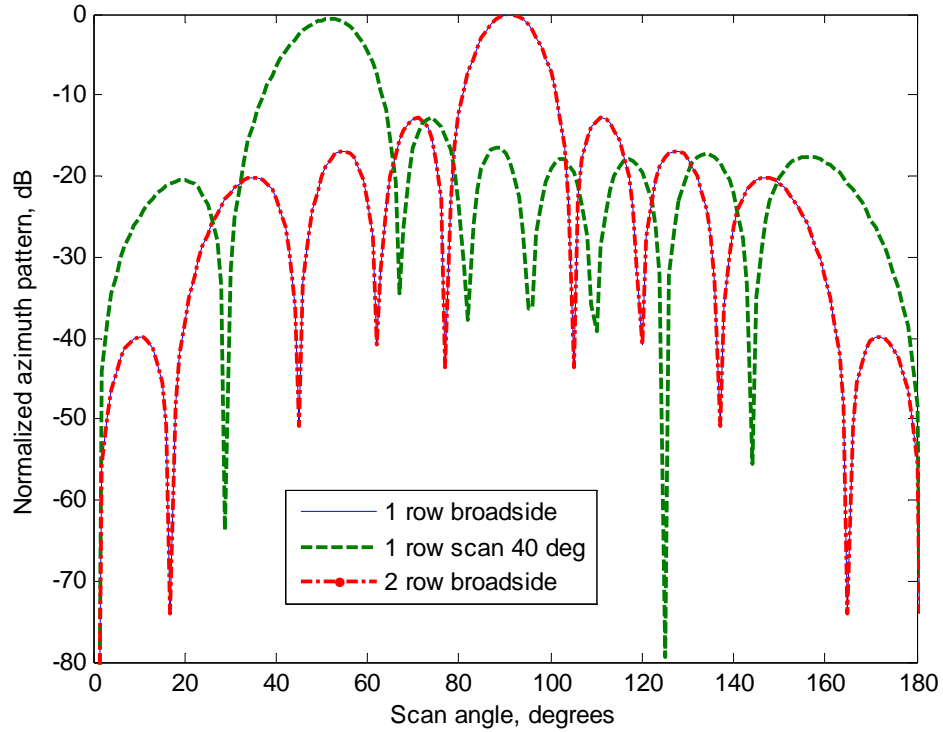
Figure 18.   Azimuth (H-plane) coverage of different arrays.

27

The elevation pattern in Figure 19 is generated for the three different configurations using the same Matlab codes in Appendix B.
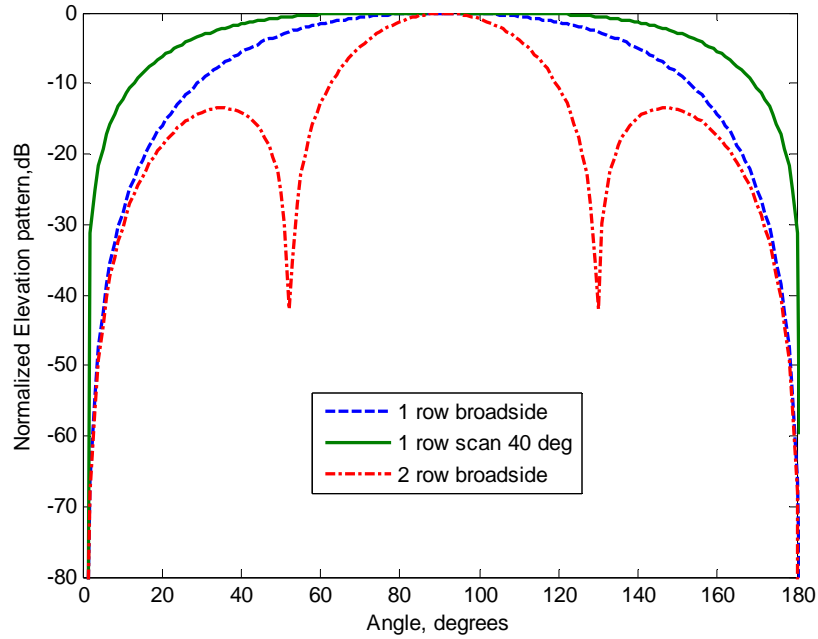
Figure 19.   Elevation (E-plane) coverage of different arrays.

This tilting of the array antenna will reduce the multipath effects and the reflections from the earth. The null region and first sidelobe of the elevation pattern for the 2 row array is pointed at the ground, which reduces reflections. Due to the constraint on the size of the dipole cards, the closest *x*-direction element spacing is 10 cm. Although by adding 8 more elements, the signal-to-noise ratio (SNR) can be increased by a factor of 8, this is not an overwhelming advantage as the transmitter power of the UAV is sufficiently high.

B.   SUM AND DIFFERENCE BEAM MATLAB RESULTS COMPARED WITH CST MICROWAVE STUDIO RESULTS

The results, using the formulas in Matlab codes for the sum and difference beams will be compared with those generated by CST Microwave Studio from the thesis by Gezer [2]. The reason for comparing the Matlab results with the CST Microwave Studio is to verify that the Matlab results are close to the CST Microwave Studio results, as CST

Microwave Studio includes the effects of the ground plane edges and mutual coupling on the patterns. It also has the exact dipole circuit modeled, which gives the proper element factor.

CST Microwave Studio is a software package for electromagnetic analysis and design in the high frequency range. The Finite Integration Technique (FIT), a time-domain numerical method based on the integral form of Maxwell's equations, is used in CST Microwave Studio. The parameters of the device that is modeled can be defined in detail in three dimensions. The program is especially suited to the fast efficient analysis and design of components like antennas, filters, transmission lines, couplers, connectors, printed circuit boards, resonators, etc.

The simulation model used to run the sum and difference patterns of the array of dipoles with scanning in the H-plane of the array is shown in Figure 20.
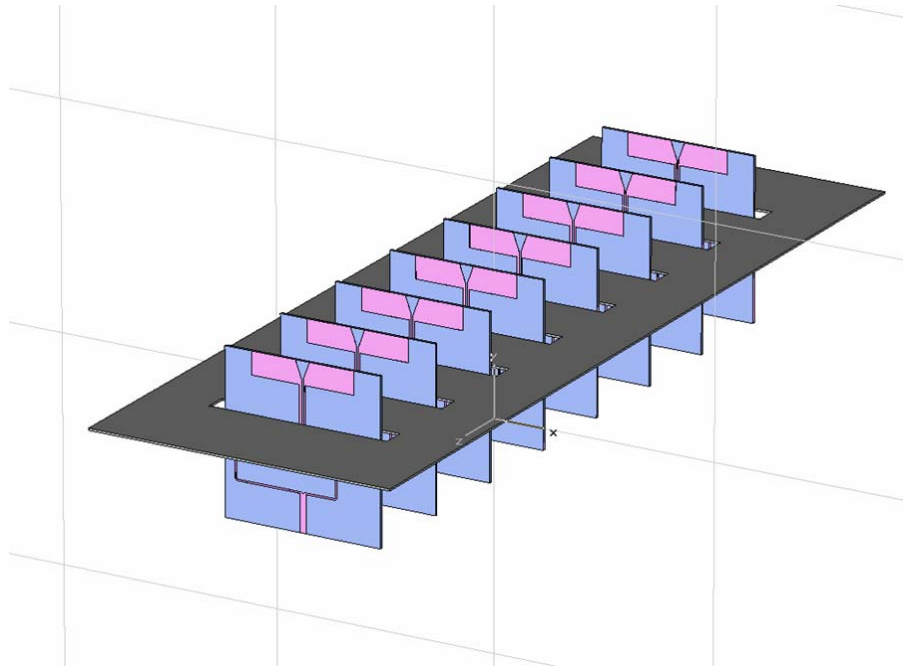
Figure 20.   Top view of the array of dipoles with ground plane modeled in CST Microwave Studio. From [2].

The Matlab codes in Appendix B are used to generate the sum and difference beam for comparison with the CST Microwave Studio. In order to compute the difference beam, AF_z in Equation (18) is modified slightly. Assuming N_z is even, for the difference beam:

$$AF_z = \sum_{m=1}^{N_z/2} A_m e^{j\beta z_m(\cos\theta - \cos\theta_s)} - \sum_{m=N_z/2+1}^{N_z} A_m e^{j\beta z_m(\cos\theta - \cos\theta_s)} \tag{29}$$

It can be seen that the array output of one-half of the array is subtracted from the output of the other half.

The H-plane comparison results of the difference and sum beam for a scan of $0°$ from broadside are shown in Figures 21 and 22, respectively. The two methods are in good agreement, except at very wide angles.
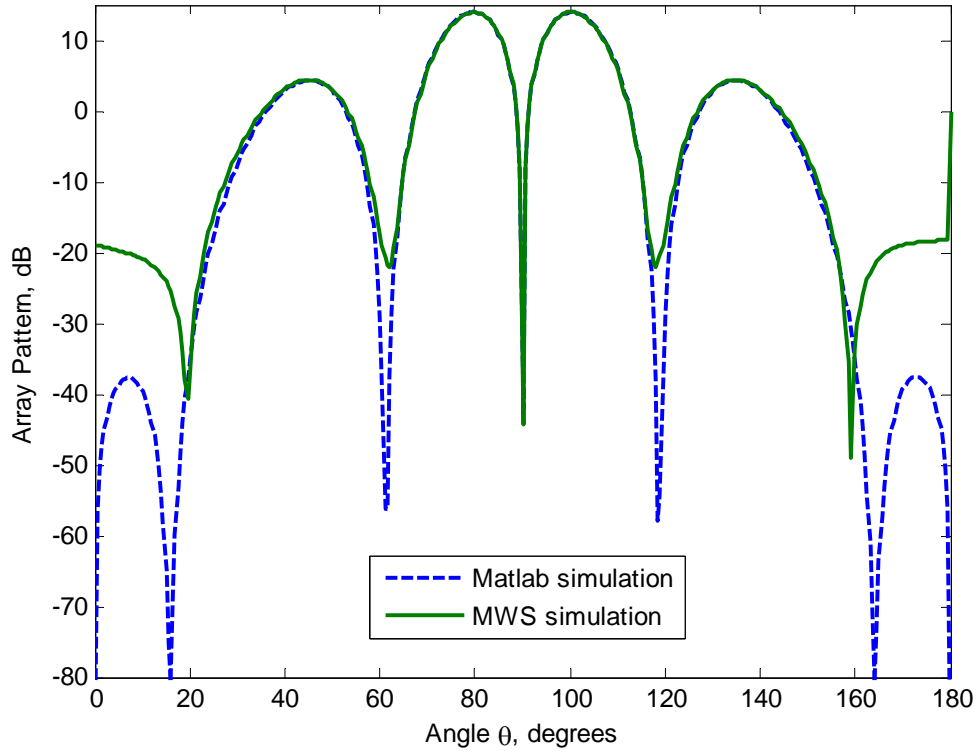
Figure 21.   Azimuth (H-plane) difference beam comparison at scan of $0°$ from broadside.
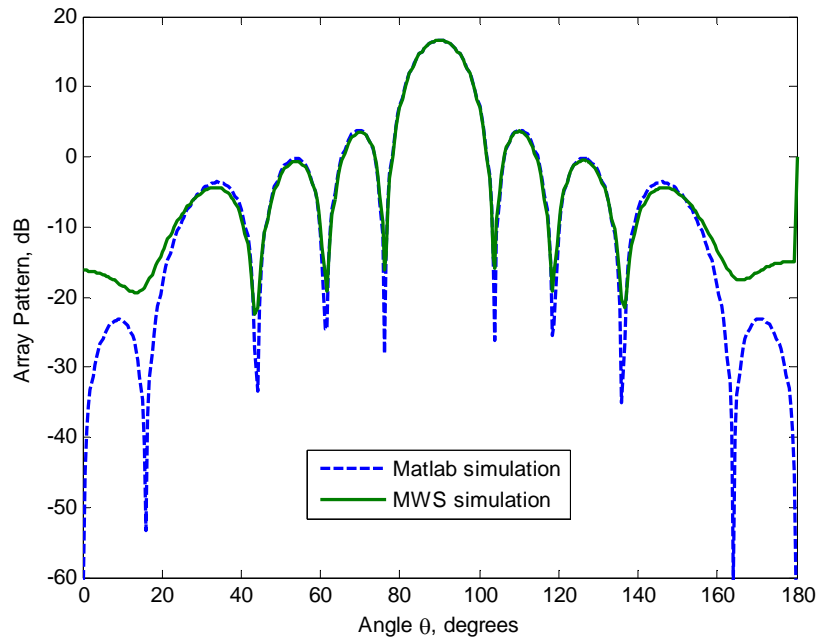
Figure 22.   Azimuth (H-plane) sum beam comparison at scan of 0° from broadside.

The H-plane comparison results of the difference and sum beam for a scan of 40° from broadside are shown in Figures 23 and 24, respectively. Again, the two methods are in good agreement.
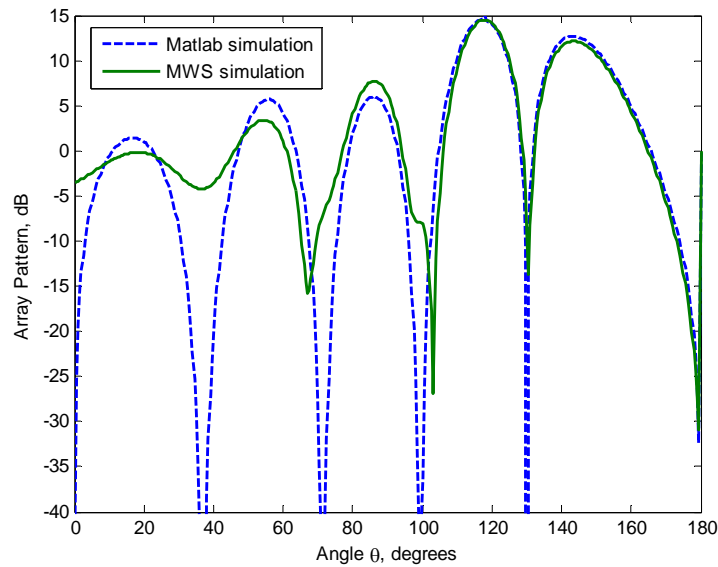
Figure 23.   Azimuth (H-plane) difference beam comparison at scan of 40° from broadside.
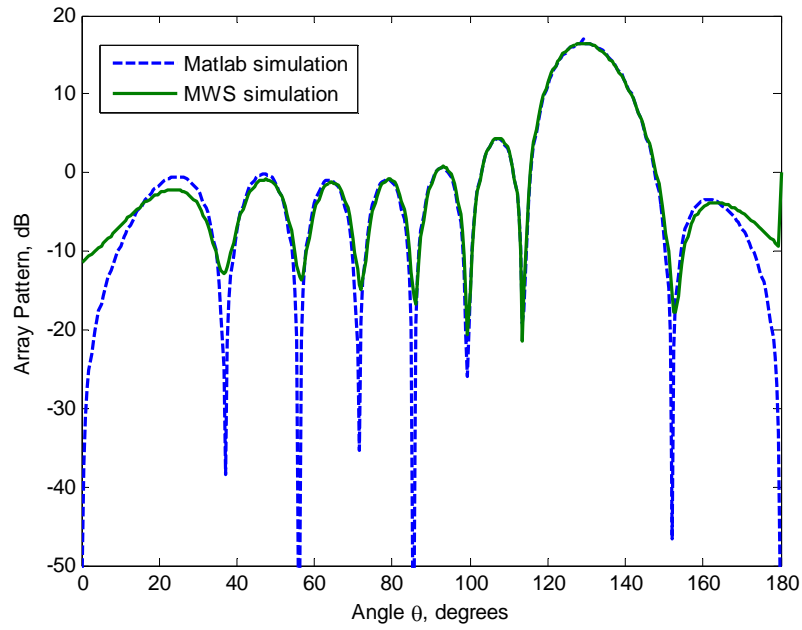
Figure 24.   Azimuth (H-plane) sum beam comparison at scan of 40° from broadside.

The E-plane comparison of results is shown in Figure 25. For the Matlab calculation, both a half-wave dipole pattern and ideal dipole pattern are shown, as described in Appendix B.
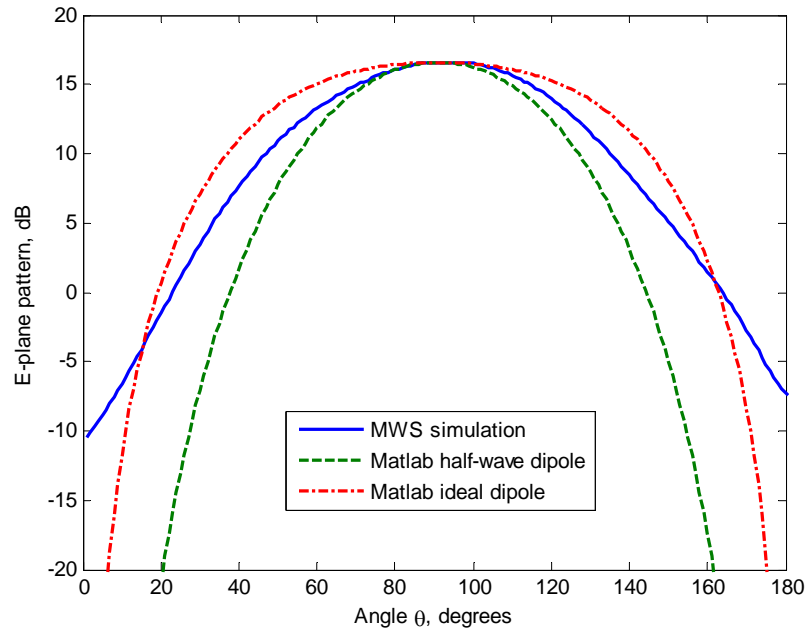
Figure 25.   Elevation (E-plane) pattern comparison.

C.   SUMMARY

The one row array is chosen primarily because the UAV will be within the HPBW for all ranges. Therefore elevation tracking is not necessary. Although the SNR can be increased by 8 times by adding a row of 8 more elements, this will add to the cost of equipment and the UAV transmitter power is sufficiently high. The azimuth and elevation patterns of the array were examined. The sum and difference beams for the Matlab simulations are in close agreement with the CST Microwave Studio simulations. The printed circuit dipole element was found to have an E-plane pattern HPBW between that of an ideal dipole and a half-wave dipole.

THIS PAGE INTENTIONALLY LEFT BLANK

IV.   FREQUENCY MODULATION (FM) DEMODULATOR

A.   INTRODUCTION

Apart from tracking the UAV, there is a requirement to recover the information from the signals transmitted by the UAV. The signal of interest will be either a NTSC video signal or audio signal, that is frequency modulated (FM) onto a 2.4 GHz carrier. The modulation characteristics of the FM video and audio signals are shown in Table 1.

Parameters	Bandwidth	FM Modulation	Modulation Index
Video and Audio	6 MHz	Wideband	>1.0
Audio	22 kHz	Narrowband	<1.0

Table 1.   Parameters of FM video and audio signals. From [22].

UAV surveillance has attempted to take advantage of cheap wireless video transmitters or receivers that operate at 2.4 GHz in the ISM band (license free band). Typical low power transmitters have power ratings in the range of 10-100 mW, although more powerful devices are available. For UAV applications, longer ranges are possible using higher power. The 2.4 GHz wireless video transmitters, which can transmit a broadcast quality picture, generally use a FM modulation method for audio/video transmission. One thing to note is that 2.4 GHz wireless video systems are not the only equipment that uses this frequency band. For example WLAN systems and microwave ovens operate at the same frequency band and can cause interference in the operation of a 2.4 GHz video link.

The output of each array element is an FM signal with a 2.4 GHz carrier. These signals need to be weighted and summed for beamforming, and then demodulated to get the video or audio. The beamforming can be done at the carrier frequency or at baseband. Either way, it is necessary that the incident wave phase change between elements is

retained for beamforming. There are several approaches to demodulating the FM signal at the antenna. Table 2 shows the types of FM detectors that are used for the demodulation of FM signals.

Name of detector	Type of detector	Circuit used
Frequency discriminator	Non-coherent	Quadrature demodulator (Bilotti) Foster-Seeley detector Balanced frequency discriminator
Phase-locked loop (PLL)	Coherent	Analog phased-locked loop
Digital sampling	Coherent	Analog-to-Digital Converter (ADC)

Table 2.   Types of FM detectors. From [24]

The ADC for demodulation of the FM signals (also known as the digital demodulator), at some point, converts the analog signal into a digital representation prior to demodulation. The most direct approach is to sample the received signal out of the antenna, but this requires a very high-speed ADC. If ten times oversampling is used (which is common), the sampling frequency would have to be $10 \times 2.4\ \text{GHz} = 24\ \text{GHz}$. The fastest ADCs today are in the 2-4 GHz range. Two common approaches to implement this are to sample at a lower intermediate frequency (IF), e.g., around 30 MHz, or to mix the signal down to baseband, where I/Q components are required to retain all the information in the signal. The Foster-Seely detector and balanced frequency discriminator convert FM into amplitude modulation (AM) and use an AM detector to recover the message signal from the converted waveform. The quadrature demodulator converts FM into both phase modulation (PM) and AM and either type of detector can be used to recover the message signal. This is referred to as Bilotti's method.

A local oscillator (LO) signal is necessary for downconverting from 2.4 GHz to baseband. The LO signal can be provided by an oscillator at the antenna, or by extracting

(recovering) the carrier from the received signal. Each of these methods has advantages and disadvantages. A phase-locked loop (PLL) is one way to recover the carrier. A PLL is an electronic control system that generates a signal that has a fixed relation to the phase of a "reference" signal. A phase-locked loop circuit responds to both the frequency and the phase of the input signals, automatically raising or lowering the frequency of a controlled oscillator until it is matched to the reference in both frequency and phase [25]. If the analog signal processing, prior to sampling into the digital domain, is done with phase-locked sources, the digital demodulator can support either coherent or non-coherent demodulation. This is a key potential benefit of the digital solution [26].

Several of the methods for the demodulation of the FM signals will be examined to assess their applicability to the tracking array.

B.   LOCAL OSCILLATOR AND DEMODULATION APPROACHES

Three FM demodulation methods are briefly explained in this section. A closely related issue is how the local oscillator signal is generated. The LO signal can be extracted from the incoming signal or generated locally. Both of these methods may require feedback to keep the LO locked on the incoming carrier.

1.   Phase Locked Loop

A PLL is a control circuit that is capable of acquiring a signal and locking on to it. The PLL system consists of three parts: phase comparator, low-pass filter (LPF), and voltage-controlled oscillator (VCO). All parts are connected to form a closed-loop frequency-feedback system, as shown in Figure 26.
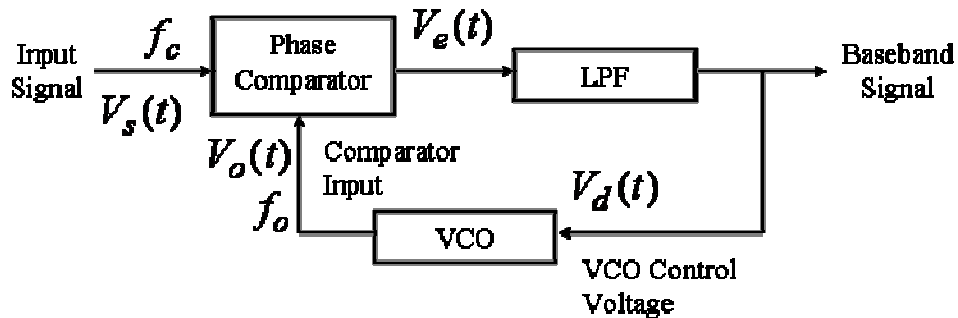

Figure 26.   PLL Block Diagram. From [27].

With no signal input applied to the PLL system, the error voltage at the output of the phase comparator is zero. The voltage, $V_d(t)$, from the LPF also is zero, which causes the VCO to operate at a set frequency, f_o, called the center frequency. When an input signal is applied to the PLL, the phase comparator compares the phase and frequency of the signal input with the VCO frequency. It then generates an error voltage proportional to the phase and frequency difference of the input signal and the VCO. The error voltage, $V_e(t)$, is filtered and applied to the control input of the VCO. $V_d(t)$ varies in a direction that reduces the frequency difference between the VCO and signal-input frequency. When the input frequency is sufficiently close to the VCO frequency, the closed-loop nature of the PLL forces the VCO to lock in frequency with the signal input; i.e., when the PLL is in lock, the VCO frequency is identical to the signal input, except for a finite phase difference. The range of frequencies over which the PLL can maintain this locked condition is defined as the lock range of the system. The lock range always is larger than the band of frequencies over which the PLL can acquire a locked condition with the signal input. This latter band of frequencies is defined as the capture range of the PLL system [27].

2.   Local Oscillator With No Feedback

Using an independent LO with no feedback is similar to a PLL in the free running mode, as shown in Figure 27. Ideally the VCO frequency should be exactly the same as the carrier frequency, f_c. If not, then the reference for frequency demodulation will be off. If the carrier frequency of the transmitter is stable and accurate and the VCO frequency is also stable and accurate, then the baseband signal can be demodulated. In the next two sections, Matlab simulations are demonstrated to estimate how much frequency error between the input signal and VCO can be tolerated.
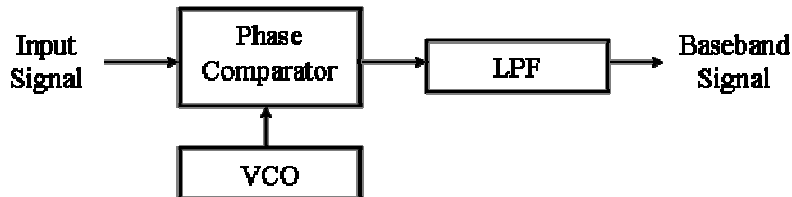
Figure 27.   Stand-alone VCO for a local oscillator.

3. Bilotti's Quadrature Demodulator[3]

The modulation of an FM signal is the deviation of a carrier from its nominal frequency. To demodulate this signal, its frequency deviation is converted to either phase or amplitude and the change in phase or amplitude is detected. In the quadrature demodulator (also called Bilotti's method), the modulated carrier is passed through an LC tank circuit that shifts the signal by 90° at the center frequency. The direction of frequency deviation will cause the phase shift to be either greater or smaller than 90°. The LC tank circuit simultaneously converts the FM to amplitude modulation (AM), so an amplitude detector could also be used.

Bilotti's quadrature demodulator uses a phase shift network and a phase detector, as shown in Figure 28 [29].
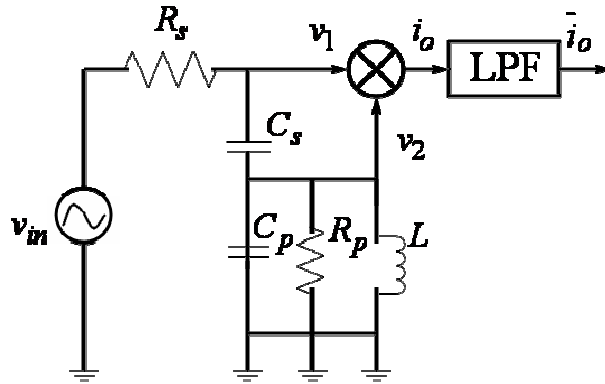
Figure 28.   Quadrature demodulator block diagram. From [29].

The signal out of the antenna is v_{in}. The phase detector compares the phase of the input signal (v_1) to v_2, the signal generated by passing v_1 through a phase shift network. This phase shift network includes an LC tank (L, R_p and C_p) and a series reactance (C_s). The network gives a frequency-sensitive phase shift. The phase detector discussed is the bipolar, double-balanced multiplier popularized by Bilotti. The output of the multiplier ($\bar{i}_o$) is filtered, which results in a DC level that changes as the input frequency changes.

---

[3] Much of this material in section A and B is from [29].

To derive the transfer function of the quadrature demodulator, the phase shift network is drawn as a small-signal circuit model in Figure 29.
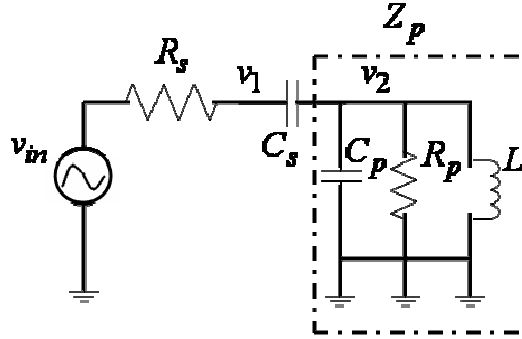
Figure 29.   Small signal model of the quadrature phase-shift network. From [29].

The impedance (Z_p) of the parallel combination of L, R_p and C_p is:

$$Z_p(s) = \frac{R_p Ls}{C_p R_p Ls^2 + Ls + R_p} \tag{30}$$

where $s = j\omega$. The ratio of v_2 over v_1 is the ratio of impedances $Z_p(s)$ over $(Z_p(s) + 1/sC_s)$. Simplifying this ratio gives:

$$\frac{v_2}{v_1} = \frac{C_s Ls^2}{(C_p + C_s)Ls^2 + \dfrac{L}{R_p}s + 1} \tag{31}$$

Equation (31) is used in the Matlab code in Appendix C to generate the plot of the phase angle versus the frequency. The resonant frequency ω_n of this filter is:

$$\omega_n = \frac{1}{\sqrt{L(C_s + C_p)}} \tag{32}$$

C.   SIMULATION RESULTS

In this section, simulation results are presented for several FM demodulation techniques.

1.   Quadrature Detector (Bilotti's Method)

In Bilotti's quadrature detector, the output can be applied to either an AM or PM detector. In the present application, the mixer and filter in Figure 28 are incorporated in the AD8347. The output $\bar{i}_o$ is in I/Q format. The demodulation is done in a computer using the sampled I/Q data. Therefore, either AM or PM could be used to recover the video signal.

Equation (31) and the Digikey catalog [30] are used to compute and select the appropriate values for the capacitances C_p and C_s and inductance L to obtain a carrier frequency of 2.4 GHz. Using off the shelf values of C_p and C_s, both are 5 pF. From available off the shelf values of L, 45 nH gives the exact carrier frequency of 2372.542 MHz. These lumped element values are used in the simulations.

Using the Matlab codes in Appendix C and varying the values of R_p, various plots for the 6 MHz video bandwidth are obtained as shown from Figures 30 to 33.

Figure 30.   Magnitude of $\dfrac{v_2}{v_1}$ plot at R_p =560 Ω , 1000 Ω and 1500 Ω .
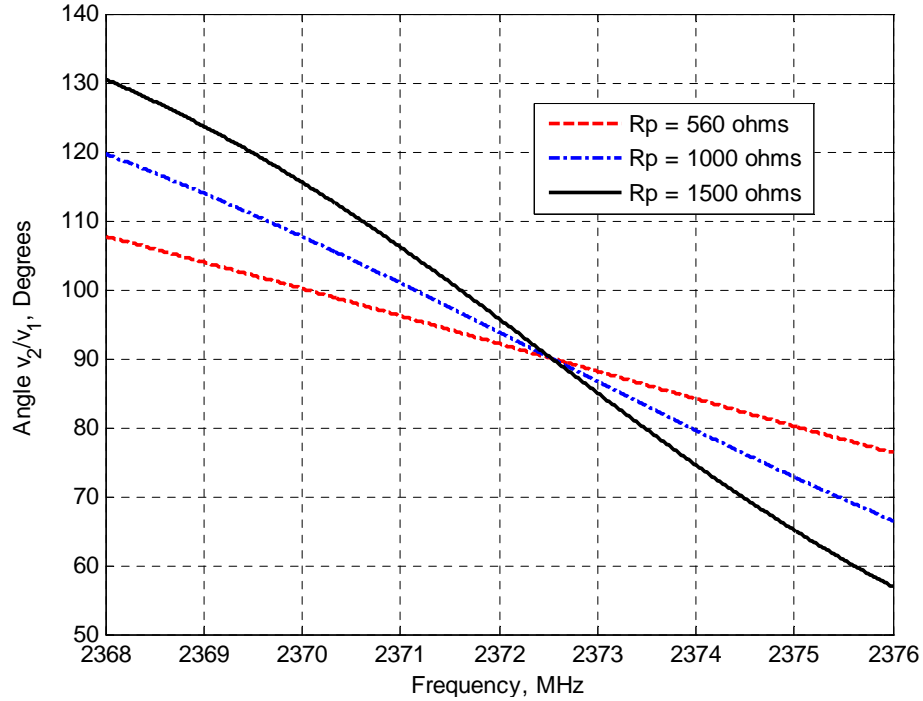
Figure 31.   Angle of $\dfrac{v_2}{v_1}$ plot at R_p =560 Ω , 1000 Ω and 1500 Ω .
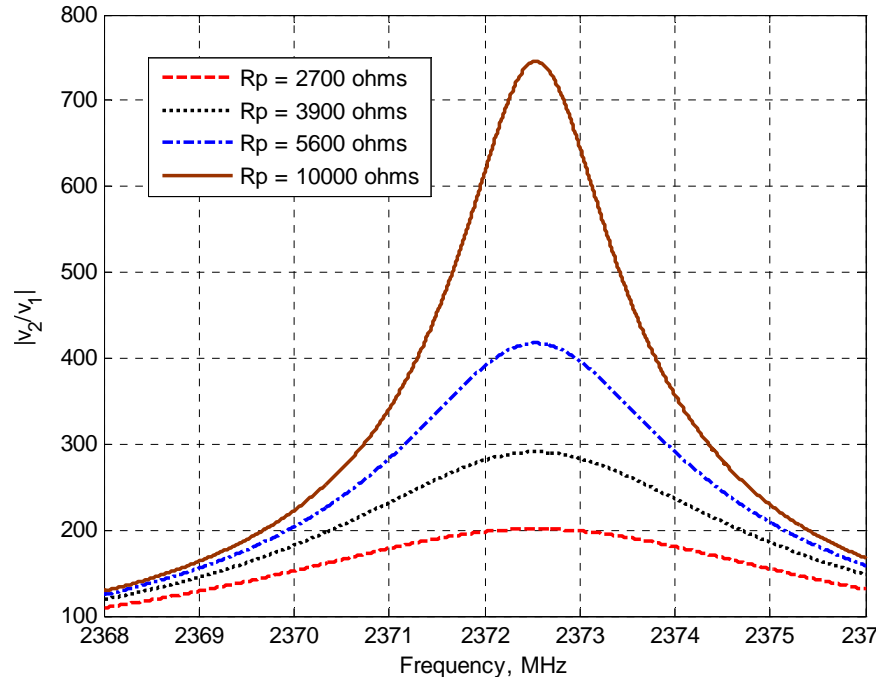
Figure 32.   Magnitude of $\dfrac{v_2}{v_1}$ plot at $R_p = 2700\ \Omega$, $3900\ \Omega$, $5600\ \Omega$ and $10\ \mathrm{k}\Omega$.
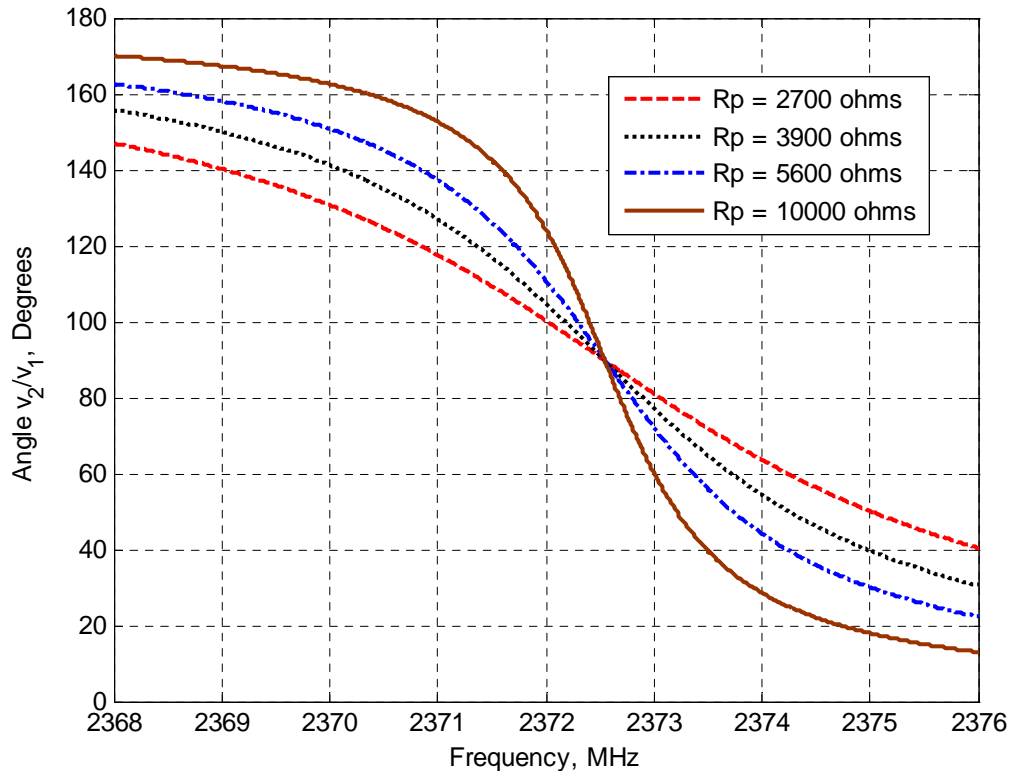
Figure 33.   Angle of $\dfrac{v_2}{v_1}$ plot at $R_p = 2700\ \Omega$, $3900\ \Omega$, $5600\ \Omega$ and $10\ \mathrm{k}\Omega$.

It can be observed that as R_p increases, more phase angles can be covered within the 6 MHz bandwidth about the carrier frequency of 2372 MHz. However, the plots become more and more non-linear. The characteristics are summarized in Table 3 for the 6 MHz bandwidth at about 2372 MHz.

R_p, Ω	Angle range,°	Behaviour
560	80 to 104	Linear
1000	71 to 114	Linear
1500	64 to 123	Linear
2700	51 to 140	Non-linear
3900	40 to 150	Non-linear
5600	29 to 157	Non-linear
10000	20 to 166	Non-linear

Table 3.   Summary of the plots in Figures 30 to 33.

If the computer processor uses AM, then a large dynamic range in amplitude is best. However, if PM is used then a linear phase curve over a large range of angles is best.

Using the Matlab codes in Appendix C and varying the values of R_p, various plots for the 22 kHz audio bandwidth are obtained, as shown in Figures 34 to 37.
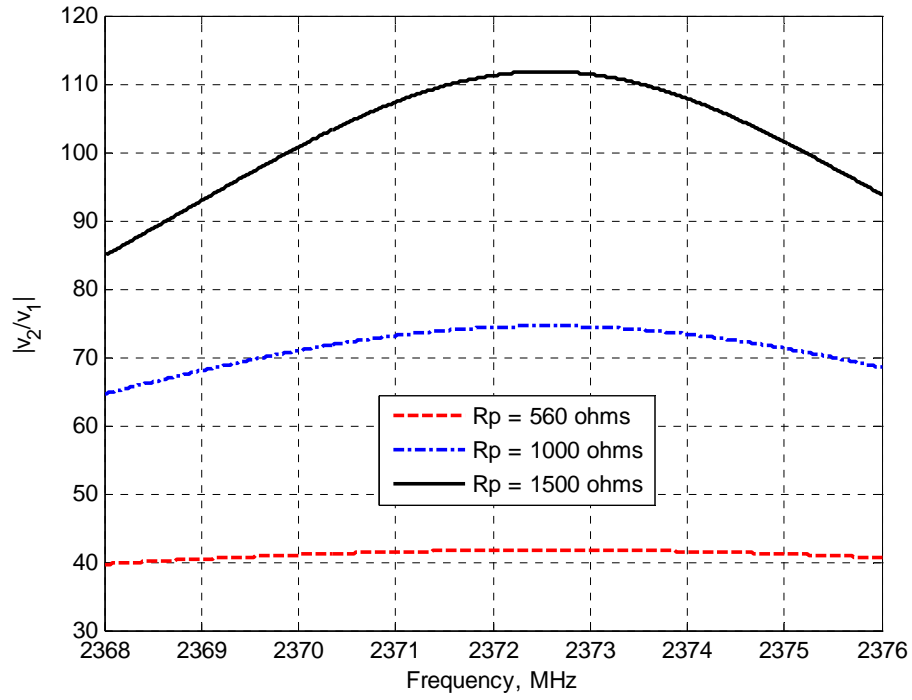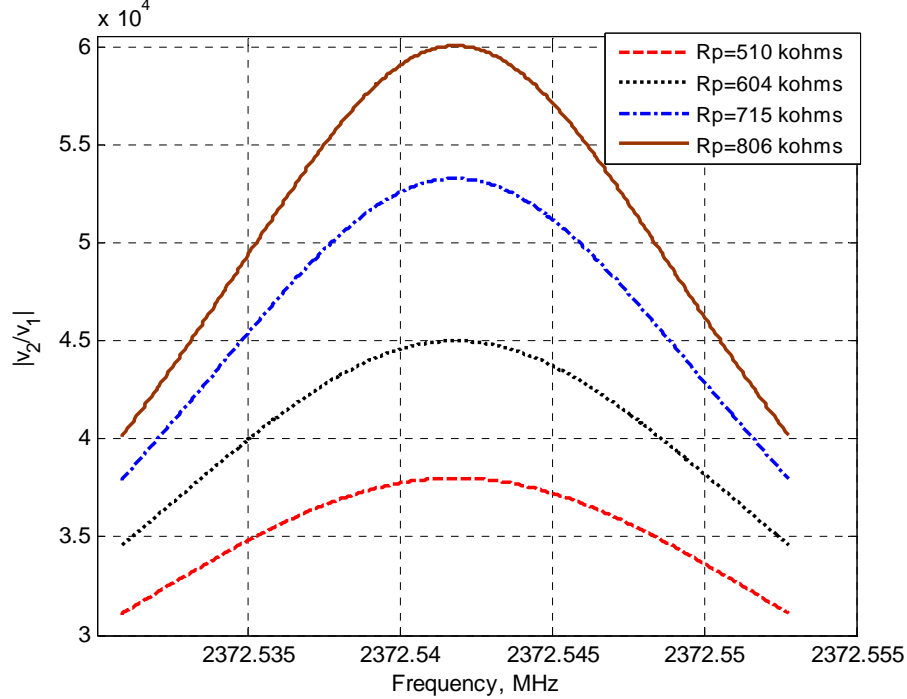

Figure 34.   Magnitude of $\frac{v_2}{v_1}$ plot at R_p =510 kΩ, 604 kΩ, 715 kΩ and 806 kΩ.

44
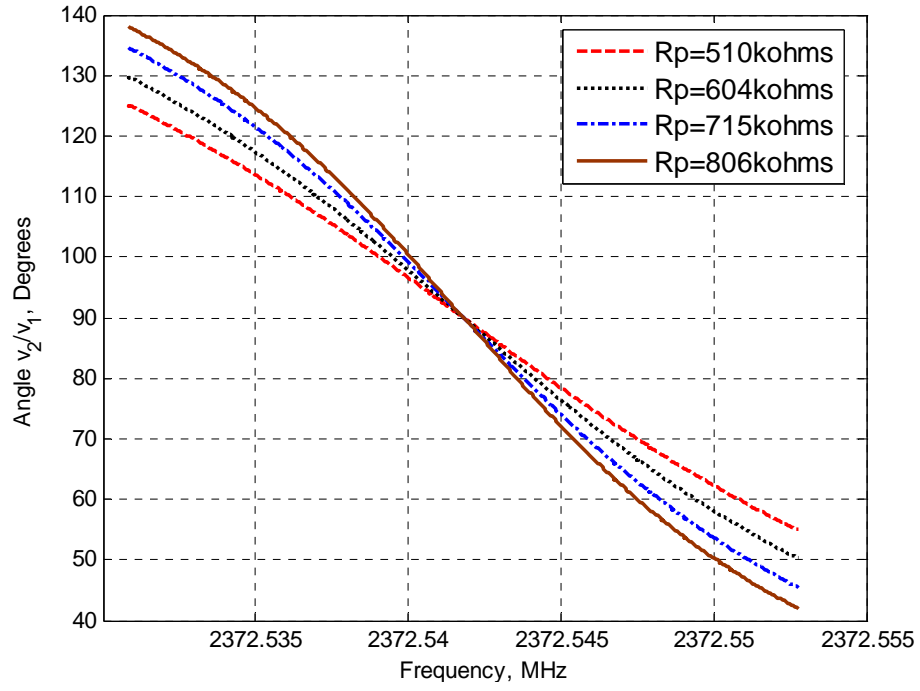
Figure 35.   Angle of $\dfrac{v_2}{v_1}$ plot at R_p =510 kΩ, 604 kΩ, 715 kΩ and 806 kΩ.
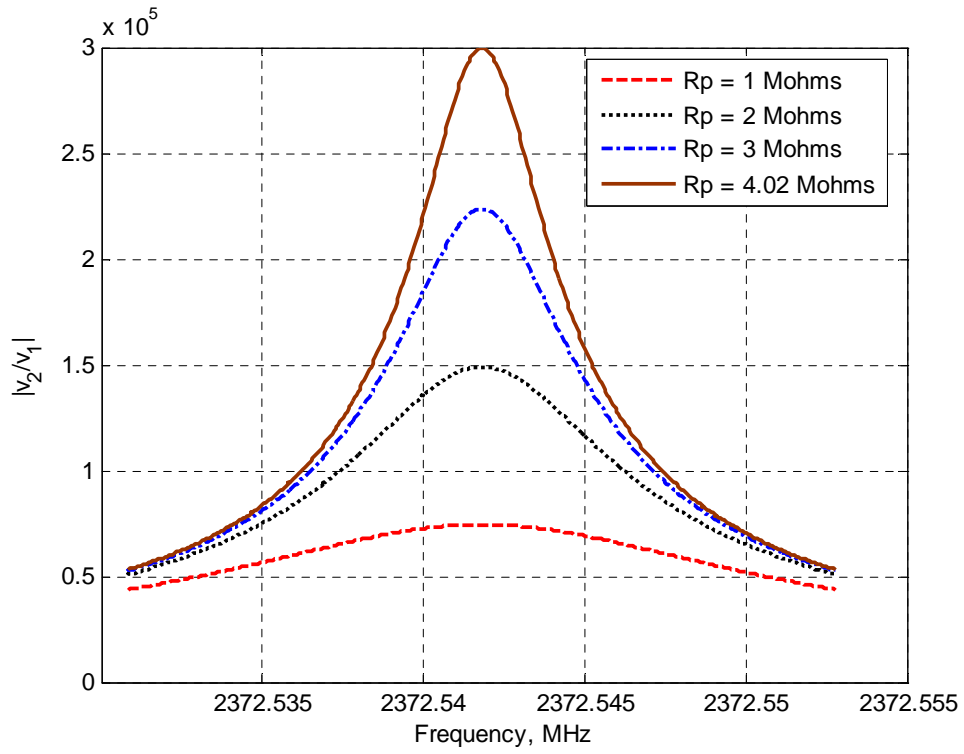
Figure 36.   Magnitude of $\dfrac{v_2}{v_1}$ plot at R_p =1 MΩ, 2 MΩ, 3 MΩ and 4.02 MΩ.
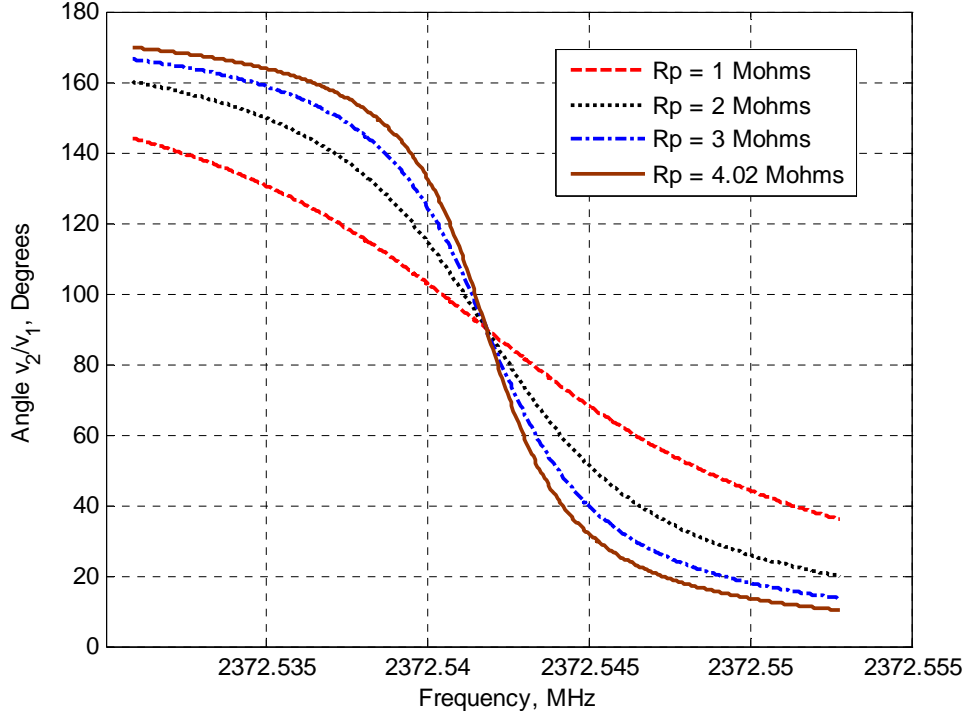
Figure 37.   Angle of $\dfrac{v_2}{v_1}$ plot at R_p =1 MΩ, 2 MΩ, 3 MΩ and 4.02 MΩ.

It is noted that as R_p increases from 510 kΩ to 4.04 MΩ, the higher values cover a larger range of phases, but the non-linear characteristic becomes more obvious. For the 22 kHz bandwidth, R_p is chosen to be 1 MΩ.

The quadrature circuit could be implemented in the digital array, as shown in Figure 38. The reference signal can be obtained using a special auxiliary antenna, or it could be tapped off of one of the elements. However it is done, the same LO source must be used for all elements.
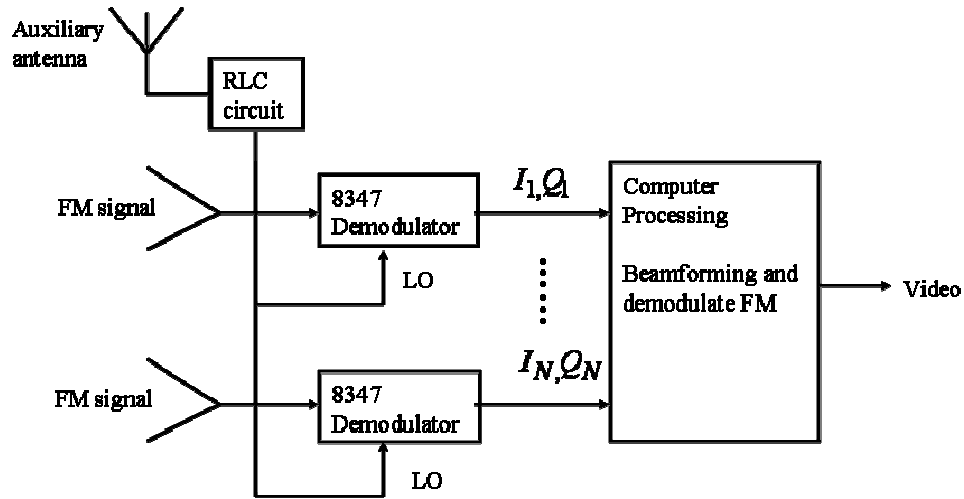
Figure 38.　Digital array using a quadrature detector.

Figure 39 shows a Matlab Simulink model for the array in Figure 38, up to the computer block. A two-tone signal, one sine wave at 900 Hz and another at 1700 Hz, is used as a source that is converted to FM. The simulation operates at 50 kHz, rather than 2.4 GHz, to greatly reduce the simulation time. The frequency deviation of the FM is set at 1000 Hz, which gives a 0.5 modulation index, assuming a maximum modulating frequency of an FM signal is 2000 Hz. A sampling frequency, which is 10 times the simulation frequency, is used to obtain a more refined simulation result. The same sampling frequency will be used for subsequent models in this section. The RLC circuit is modeled by its transfer function, and its resonant frequency was set to 50 kHz.
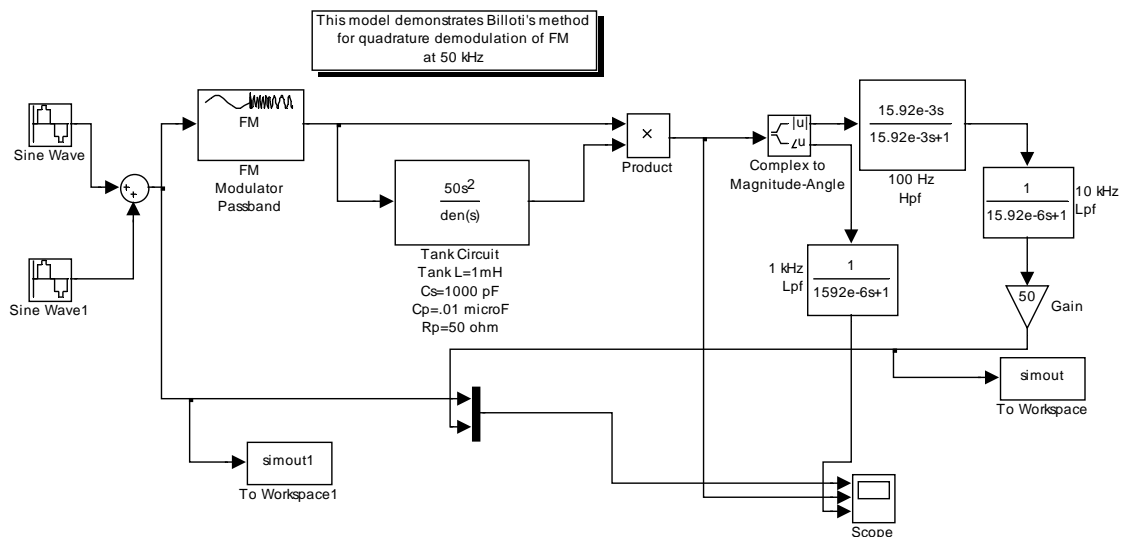
Figure 39.　Simulink model of Bilotti's quadrature demodulator.

47

The FFT of the source and recovered signals are shown in Figure 40. The frequency components of the two-tone signal are clearly visible in the recovered signal. This shows that the source signal can be recovered using Bilotti's method.
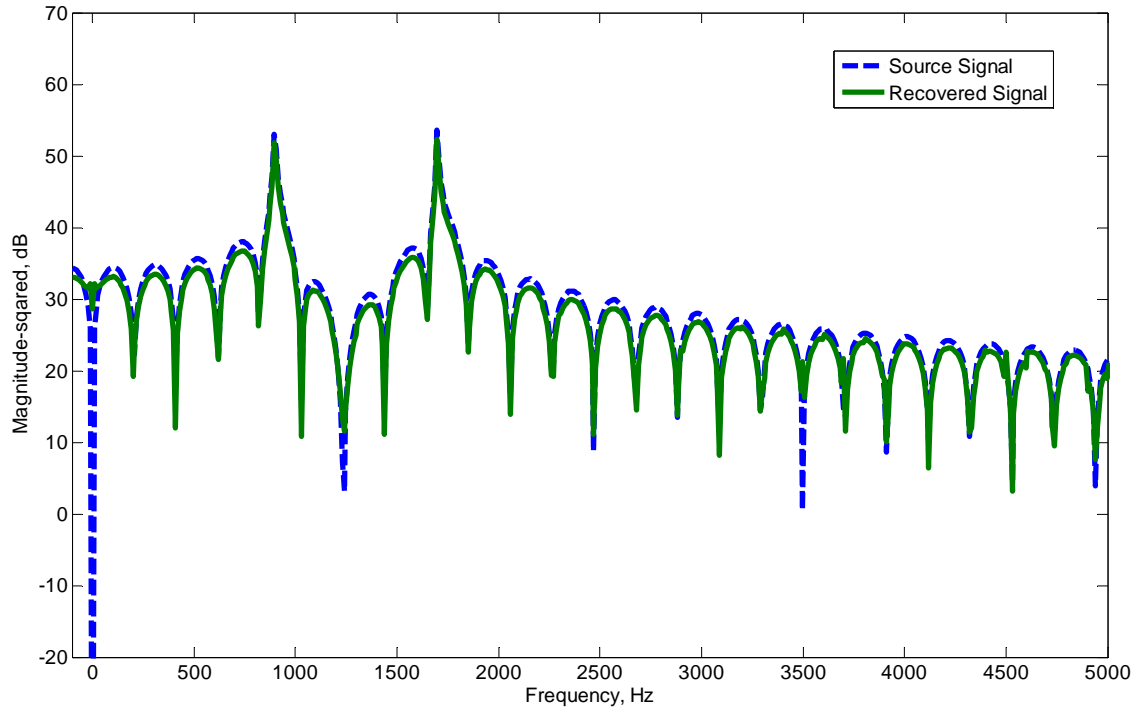
Figure 40.   FFT of the recovered and source signals in Bilotti's simulink model.

2.   Local Oscillator With No Feedback

Figure 41 shows the block diagram for an array with an independent LO. The LO will synchronize the AD8347 demodulators. As this is a method without feedback, simulations are done to consider the effects of a phase drift in the LO. The raw I and Q components from the AD8347 demodulators are processed to perform the beamforming and demodulate the FM video signal. The carrier frequency of 50 kHz with a 1 kHz deviation is used in the simulation for the modulator for transmitting the two-tone signals. Figure 42 is the Simulink model of Figure 41.

48
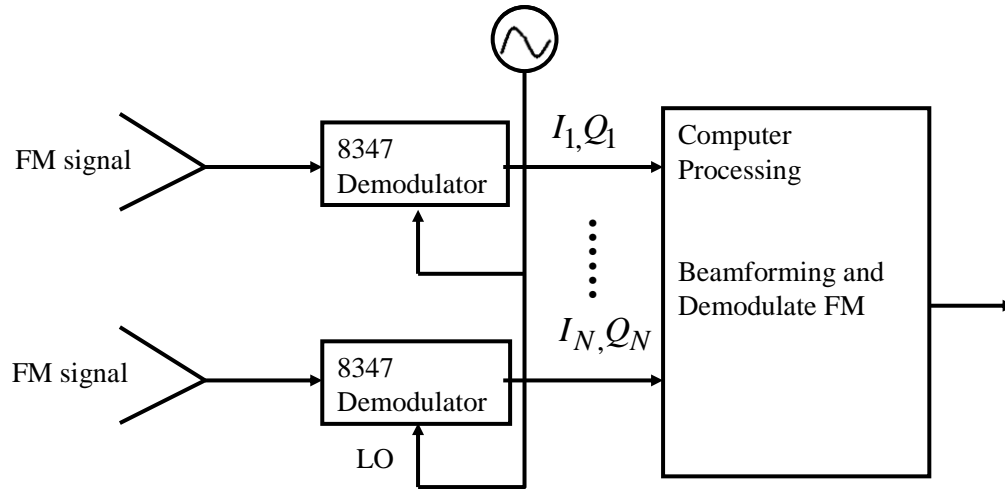
Figure 41.   Open loop digital quadrature detector.
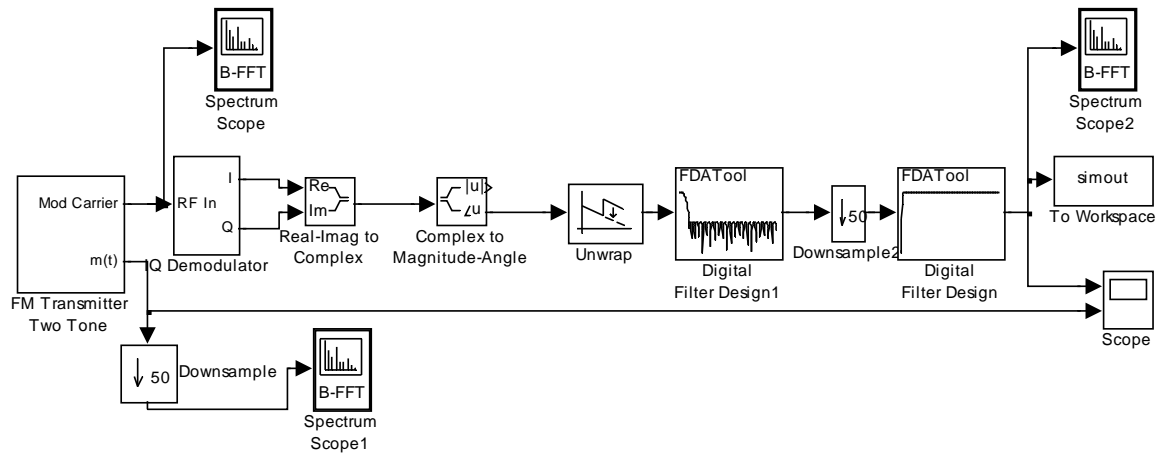
Figure 42.   Simulink model of open loop digital quadrature detector.

Figure 43 shows the input and demodulated signals in the time domain. Figure 44 shows their spectra in the frequency domain. The recovered signal matches the source signal in both the time scope and the FFT spectrum scope.
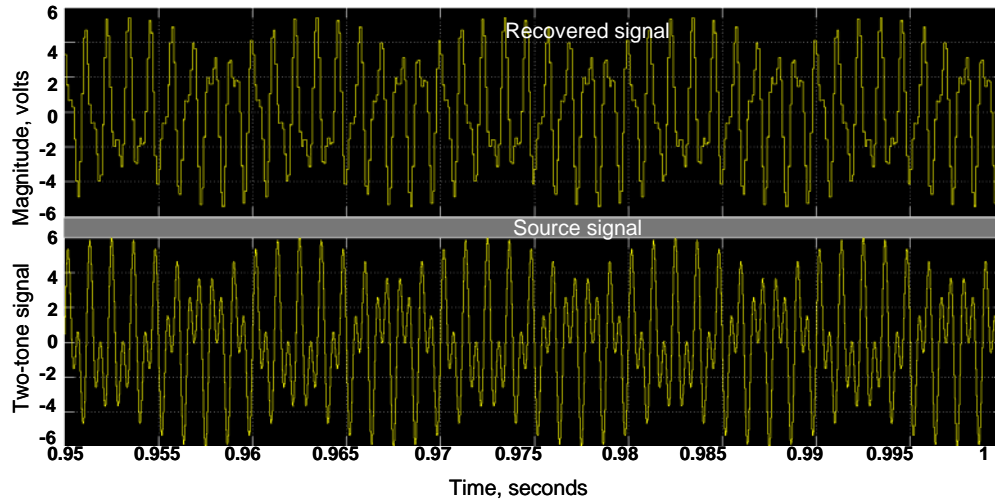
Figure 43.   Time scope of the open loop digital quadrature detector in Simulink.
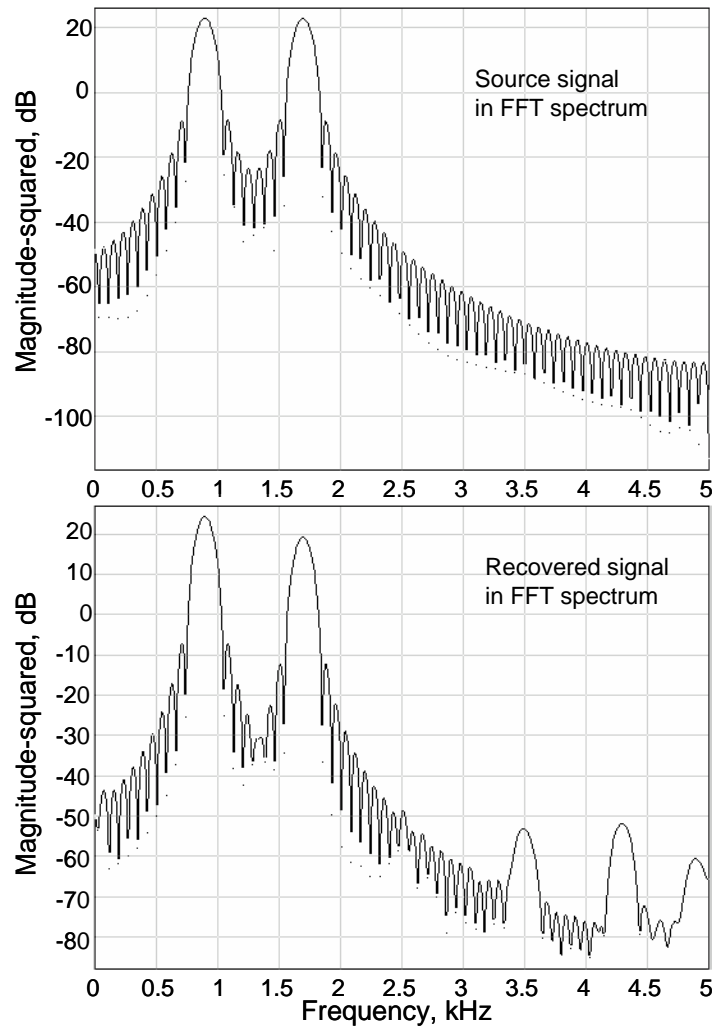
Figure 44.   FFT spectra of the source and recovered signals.

50

3. Digital PLL Quadrature Detector

Figure 45 shows how the PLL is integrated into the digital array to perform the beamforming and the FM demodulation. The output I and Q components are converted to the digital format to be processed in the computer. In the computer, the digital I and Q signals are low pass filtered before performing the beamforming and FM demodulation The error signal is computed and fed to the variable control oscillator (VCO) to adjust the VCO frequency. The same PLL is used for mixing all the elements from the other channels.
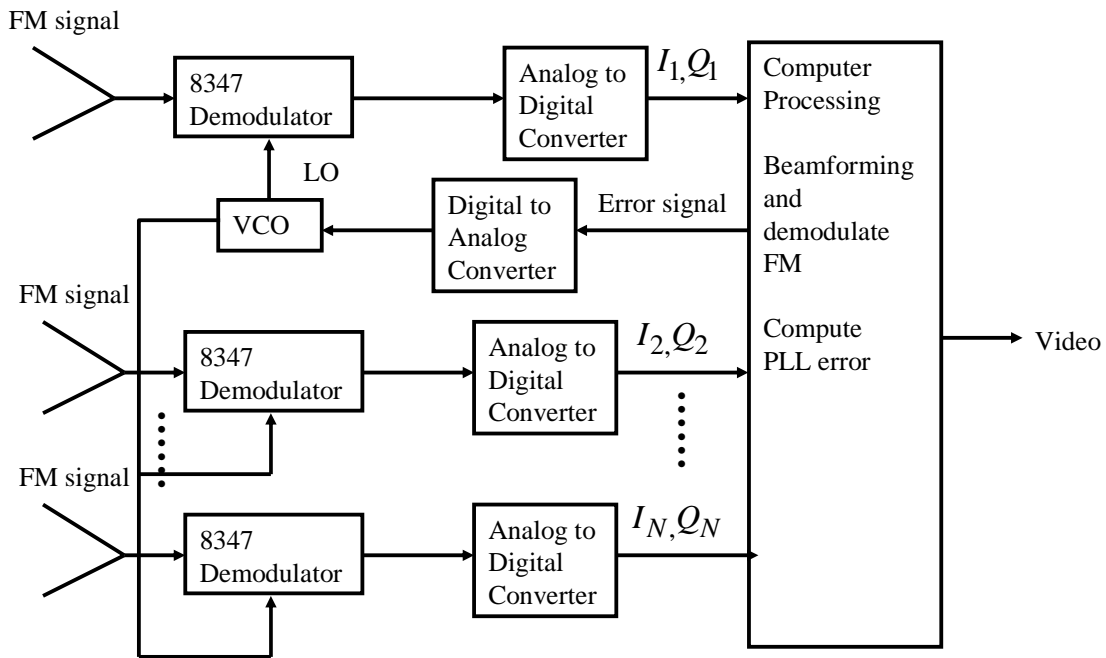
Figure 45.   Digital PLL quadrature detector.

The Simulink model in Figure 46 was used to simulate the digital PLL quadrature detector in Figure 45. The carrier frequency of 50 kHz with a 1 kHz deviation is used for the modulator for transmitting the two-tone signals. The VCO with the following parameters is inserted in the feedback loop: output amplitude of 3 V, quiescent frequency of 50 kHz, input sensitivity of 500 Hz/V and a sampling frequency of 500 kHz.

51
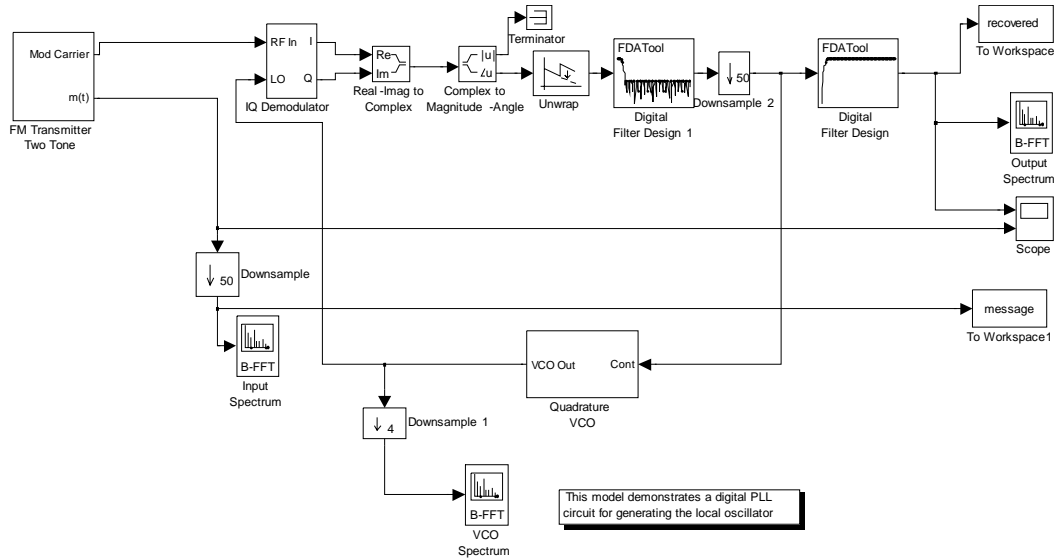
Figure 46.   Simulink model of digital PLL quadrature detector.

Figure 47 shows the input and demodulated signals in the time domain. Figure 48 shows their spectra in the frequency domain. It is noticed that the source signal matches the recovered signal for the digital PLL quadrature detector.
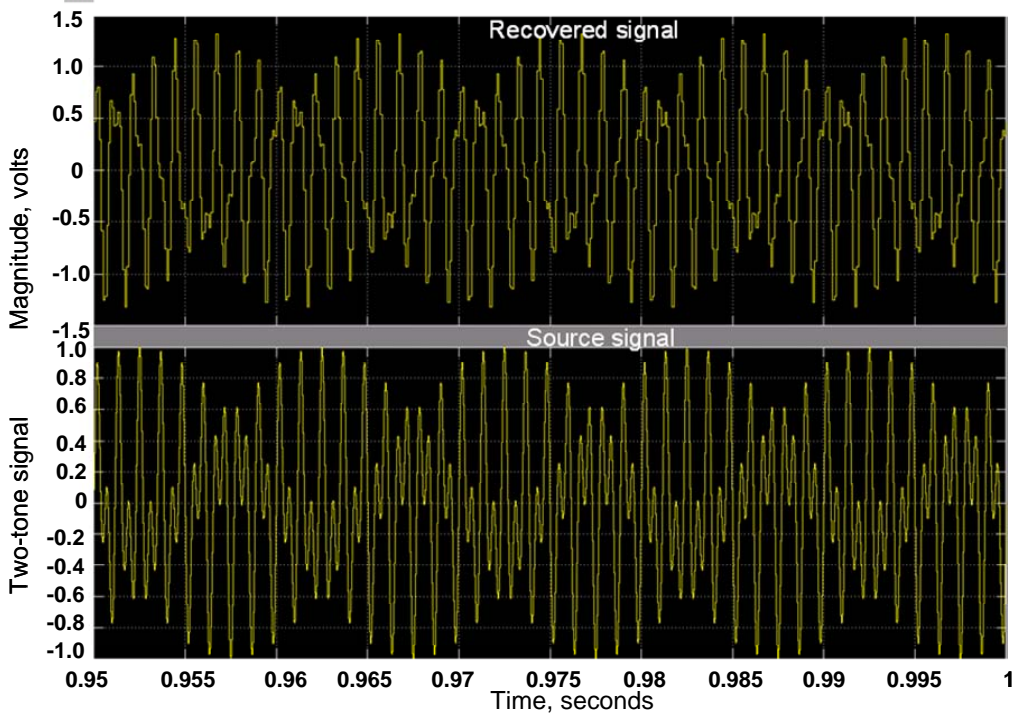
Figure 47.   Time scope of the digital PLL quadrature detector in Simulink.
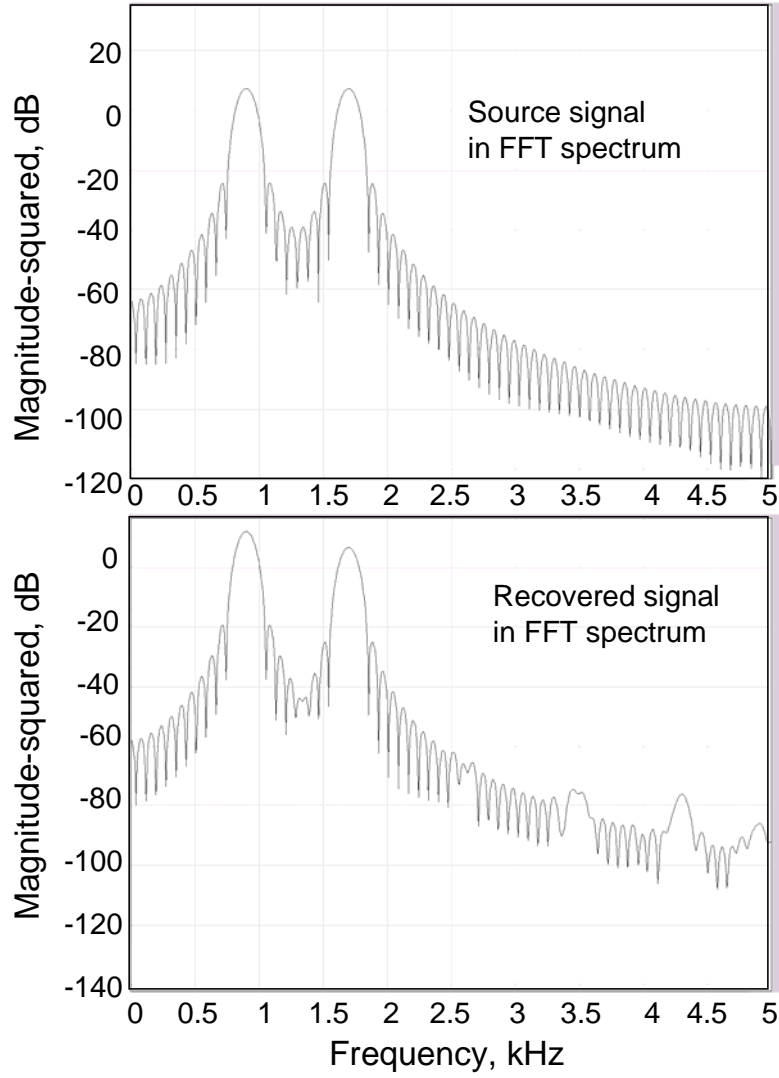
Figure 48.　FFT spectrum of the digital PLL quadrature detector in Simulink.

D.　PHASE ERRORS AND LO FREQUENCY DRIFT

There is a need to study the effects of the frequency drift in the LO and the relative phase errors in the array channels. The relative phase errors cause beamforming errors, which lead to tracking errors. In this section, the effects of phase errors of a 4-channel array modeled in Simulink are shown. The frequency drift in the LO is also simulated.

1. Relative Phase Errors in the Array Channels

The Simulink block diagram designed to model the phase errors in the array channels is shown in Figure 49 below. The carrier frequency of 50 kHz with a 1 kHz deviation is used in the simulation for the modulator for transmitting the two-tone signals. Phase shifters are introduced to the open loop digital quadrature detector Simulink model. Different delay line sizes are introduced to the other three channels to model the effects of phase shifters on the incoming signal. Ideally, the delays cause the sum output to have a maximum at the signal angle of incidence. The Simulink results, shown in Figure 50, indicate that the signal could be recovered when phase shifter errors are introduced.
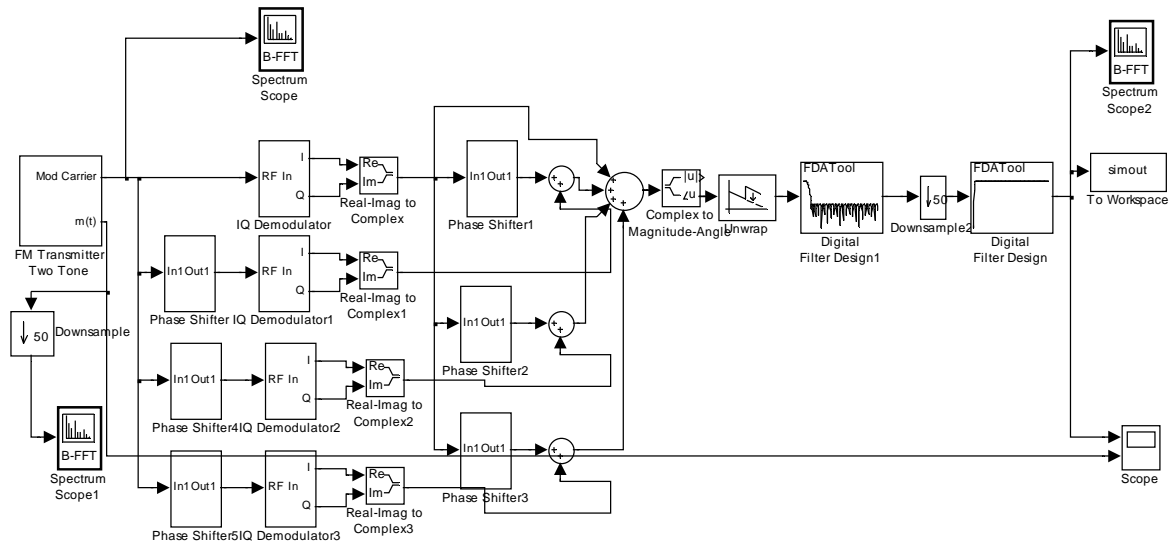
Figure 49.   Simulink model for phase errors simulation analysis.
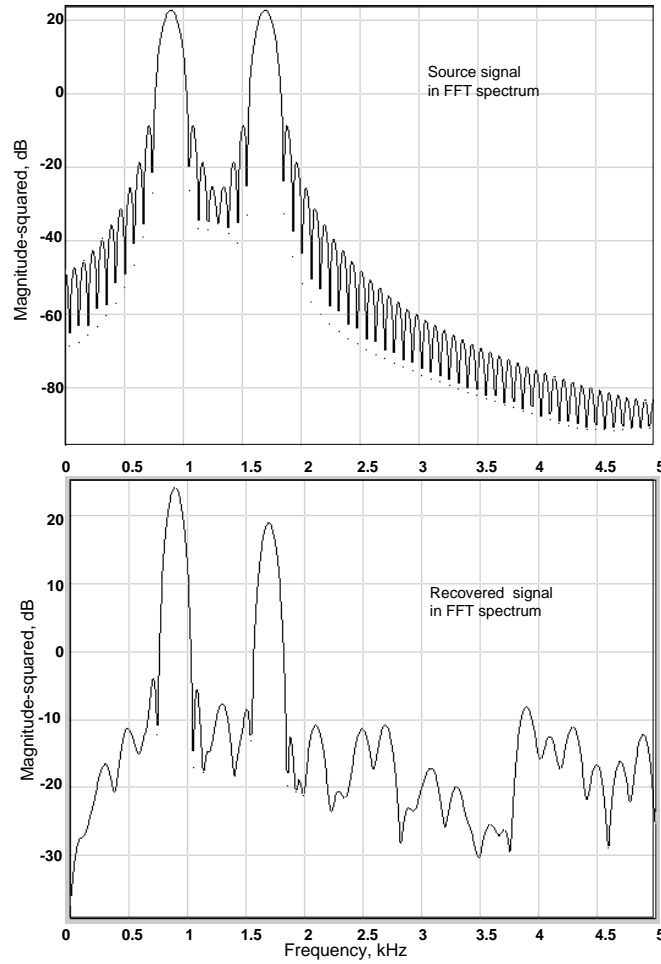
Figure 50.   Simulation results for phase errors in a 4-channel array.

2.   LO Frequency Drift

The frequency drift in the LO is simulated in the Simulink model, shown in Figure 51, at a carrier frequency of 5 MHz to analyze the effects to the recovered signal. A frequency offset of 100 Hz is introduced to the transmitter frequency.
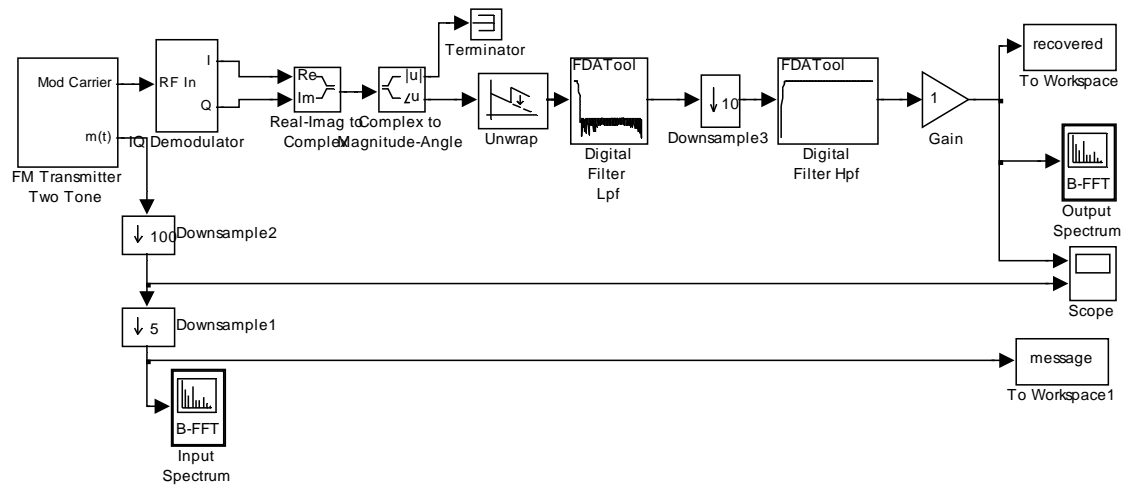
Figure 51.   Simulink model for LO frequency drift analysis.

The simulation result is shown in Figure 52.
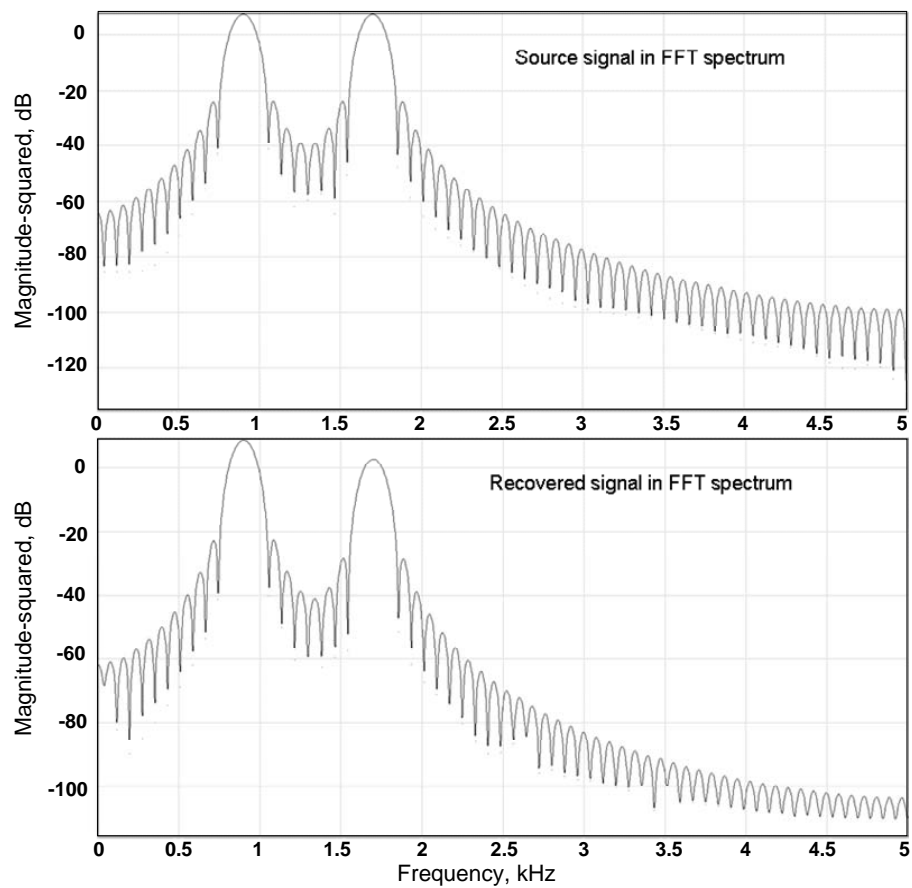
Figure 52.   Simulation result at 5 MHz with 100 Hz frequency drift.

E. SUMMARY

Simulation tools are developed for array analysis of the three FM demodulation techniques: Bilotti's method, local LO with no feedback and digital phase locked loop quadrature detector.

The LO with no feedback is preferred as it uses the least circuitry with satisfactory performance for the recovery of the two-tone signal. Beamforming can also be performed easily, as the raw I and Q data is preserved. This technique also eases the computer processing. Relative phase errors in the array channels and LO frequency drift are introduced into the Simulink model. The simulation results indicate that the recovery of the two-tone signal can still be achieved. Hence, the LO with no feedback technique can be used.

THIS PAGE INTENTIONALLY LEFT BLANK

V. SYSTEM ARCHITECTURE

This chapter discusses the hardware necessary to build the tracking array. To keep the cost down, commercial-off-the-shelf hardware is used.

A. DESCRIPTION OF TRACKING ARRAY HARDWARE

A general block diagram of a digital receiver channel is shown in Figure 53. The received FM video or audio signal undergoes the following processes:

1. Amplified by the low noise amplifier (LNA) and then fed to the RF input of an AD8347 quadrature demodulator.

2. Downconverted to baseband by the AD8347 quadrature demodulator, operating from 800 to 2700 MHz with a modulation bandwidth of about 50 MHz. The output signals are in I/Q format.

3. Sampled, filtered and then sent to the processor.

4. Processing of the detected signals is done to form the beam by combining the I/Q signals from all receive channels. The FM is removed and the video signal is recovered.

5. A common local oscillator is used to synchronize the devices to avoid phase and drifting errors between the elements.

These processes are illustrated in Figure 53.
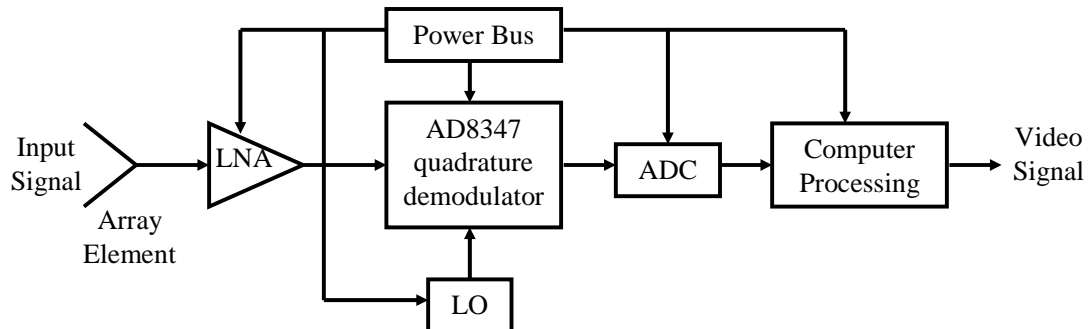
Figure 53.   Array architecture for one channel.

The dipoles, LNA, demodulator, local oscillator, power supplies, power adjustment circuit and signal processing are discussed briefly, and follow the description in Gezer [2].

1. Dipoles

The dipoles were designed in the CST Microwave Studio by Professor David C. Jenn and fabricated by Cirexx Corporation. They operate at 2.4 GHz. The return loss of the dipoles was measured and found to be at least 15 dB. Reference [8] discusses the dipole element return losses more in detail.

2. Low Noise Amplifier (LNA)

The LNA amplifies the weak signals captured by the dipoles. The LNA has a low noise figure (2.0 dB) and high gain (24 dB), which improves the performance of the array. Because the overall noise figure is dominated by the first few stages, the total noise of the cascaded stages is reduced by the LNA. Hence, the fact that the LNA has a very low noise figure is a key factor in signal detection.

The LNA must be located very close to the dipole in order to minimize the losses in the feed line. For our setup, the LNAs are connected to the dipoles with a barrel to minimize the cable loss. This SNR will be verified later in Section B. The LNA-2700 by RF Bay Inc. (shown in Figure 54) was selected as the LNA because of its reasonable price as well as its low noise figure.

Figure 54.   LNA 2700 by RF Bay Inc. From [2].

3. Demodulator

The demodulator downconverts the signal from the carrier frequency to the baseband. The demodulator selected for the array is the AD8347 Quadrature Demodulator manufactured by Analog Devices. Figure 5 shows one of these demodulators used in the system. This COTS demodulator operates within the frequency range 0.8 through 2.7 GHz and requires supply voltages between 2.7 and 5.5 V. The voltage VGIN determines the amplification of the received signal. Reference [31] includes a very detailed spec sheet of the AD8347 EVAL Quadrature Demodulator.

4. Local Oscillator

The LO is designed and manufactured by Z-Communications. The LO signal at 2.4 GHz is generated by a V800ME10 oscillator on the board and fed into the demodulators.

5. Power Supplies and Power Adjustment Circuit

The two linear power supplies used for the array are model HP 6255 A by Hewlett Packard. The power supplies provide +5 and +12 V. The +12 V is applied to VGIN of the demodulator after being adjusted with a VGIN voltage regulator, designed by Bob Broadston from NPS. The LO and LNAs are provided with +12 V by the power supply, which has maximum currents of 6.00 A, 2.50 A for the voltages of 5 V and 12 V, respectively.

6. Analog-to-digital Converters

The ADCs sample the baseband I/Q signals out of the AD8347. The minimum sampling rate is set by the baseband bandwidth, which is approximately 6 MHz for the FM video signal. For 5 times oversampling, this would be 60 MHz. For the audio signal, it would be about 110 kHz.

Candidate hardware for the audio case is the National Instruments Compact Reconfigurable I/O (cRIO) product line. The reconfigurable chassis is the heart of the NI

cRIO system and contains a Field Programmable Gate Array (FPGA). The cRIO core is powered by a user-programmable FPGA configured by a special software called LabVIEW, that serves as a high-speed interface to the I/O modules. The LabVIEW FPGA Module is used to program the FPGA on the cRIO reconfigurable chassis. FPGAs are silicon chips with unconnected logic gates. The flexible design of FPGA enables the user to target any device compatible with NI cRIO and to customize hardware functions for its system. It is possible to execute multiple tasks simultaneously using the LabVIEW FPGA module.

NI provides different I/O modules for different purposes. The four analog output signals from the demodulator are input to an analog input (A/I) module to be sampled. They are then converted into digital signals for signal processing and analysis. The A/I module selected for the audio case is the NI cRIO-9215. The NI cRIO-9215, shown in Figure 55, provides 4 simultaneously sampled analog inputs with a rate of 100 kS and a resolution of 16 bits.

Figure 55.   NI cRIO-9215 Analog Input Module. From [32].

The NI cRIO-9215 analog input modules are connected directly to the FPGA hardware. This FPGA hardware is the reconfigurable chassis NI cRIO-9104 with the real-time embedded controller cRIO-9004. The cRIO-9104 chassis has 8 slots and a RIO FPGA core with a RAM of 196 kB. The FPGA core has an individual connection to each

NI cRIO-9215 analog input module and can read information from each module. The module operation is precisely synchronized with 25 ns resolution.

B.   RECEIVER MODULE ANALYSIS

This section presents an estimate of the operating range based on the minimum power required by the demodulator (AD8347).

1.   Sensitivity and Dynamic Range

The maximum RF power that is allowed at the receiver input (without saturating it) is limited by the demodulator's 1 dB compression point (IP1dB). From [9], the demodulator's IP1dB $\approx$ -22 dBm with no Automatic Gain Control (AGC). With reference to Figure 53, the LNA gain is 24 dB and the cable losses on the two sides of the LNA are 0.2 dB and 0.4 dB. The maximum RF power that is allowable to the receiver antenna is:

$$P_{r_{\max}} = -22 + 0.2 - 24 + 0.4 = -45.4 \text{ dBm}$$

$P_{r_{\max}}$ gives the closest range without over driving the demodulator.

The minimum RF power that is required at the receiver module for operation depends on the demodulator's sensitivity. From [9], the demodulator mixer output voltage is linear with RF input power from -65 dBm to -5 dBm. Hence, with reference to Figure 53, the minimum RF power at the receiver antenna is:

$$P_{r_{\min}} = -65 + 0.2 - 24 + 0.4 = -88.4 \text{ dBm}$$

$$= -118.4 \text{ dBW} = 1.445 \times 10^{-12} \text{ W} \tag{33}$$

Hence, the dynamic range of the receiver module is $-45.4 - (-88.4) = 43$ dB.

2.   Maximum Range

Consider the distributed array block diagram in Figure 56 where

$R_n =$ the distance between the UAV and the nth receive element,

P_t = transmitted power from the UAV,

P_{r_n} = received power at n^{th} element,

G_t = gain of transmitter antenna of UAV, and

G_{o_n} = gain of receiver antenna of nth element (assume equal gains, $G_{o_n} = G_o$).
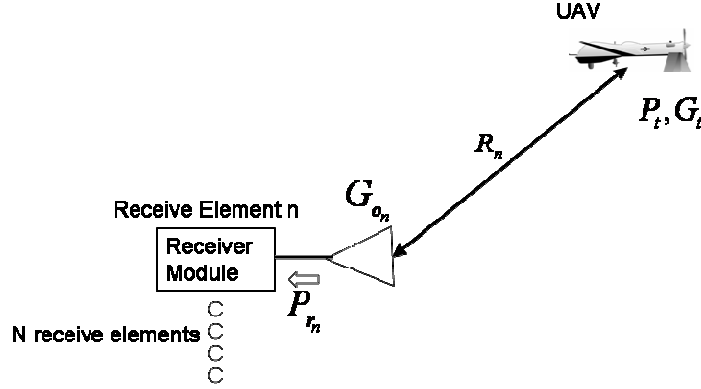
Figure 56. Distributed array of receiver antennas.

At any one time, N elements are receiving signals from the UAV, where N is the total number of elements in the array, which in our case is $N = 8$. From Figure 56, the one-way Friis equation is used to determine the maximum operating range, $R_{\max}$. It is considered that there is no polarization mismatch, input mismatch or other system losses. The one-way signal strength from a transmitter to a receiver element is:

$$P_r = \frac{P_t G_t G_o \lambda^2}{(4\pi)^2 R_n^2} \tag{34}$$

To include receiver sensitivity in Equation (34), $P_{r_{\min}}$ is used to determine the maximum range:

$$R_{\max} \cong \sqrt{\frac{P_t G_t G_o \lambda^2}{(4\pi)^2 P_{r_{\min}}}} \tag{35}$$

It will be assumed that P_t is 100 mW in this case. The gain of each of the receiver elements is G_0 and calculated to be $6.3 = 8$ dBi. Thus, substitute $P_t = 100$ mW, $G_t = 1.6$, $G_0 = 6.3$, and $P_{r_{min}} = -88.4$ dBm into Equation (35) to get $R_{max} = 8.31$ km.

C.   SUMMARY

A description of tracking array hardware was the subject of this chapter. The possible hardware components were briefly introduced. From the block diagram of the receiver module, the minimum power for the receiver module was used to determine the maximum operating range of the array using the one-way Friis equation.

THIS PAGE INTENTIONALLY LEFT BLANK

VI. CONCLUSIONS AND RECOMMENDATIONS

A. SUMMARY AND CONCLUSIONS

As a part of an ongoing project, this research's aim was to design a digital phased array for receiving and tracking a 2.4 GHz FM video signal from an unmanned air vehicle. Tracking the signal from the UAV will establish a data link for data transfer such as video, image or audio between the UAV and the ground station.

An array tradeoff study was done to determine the benefits of the 1 row and 2 row arrays with 8 elements per row in terms of HPBWs of the azimuth and elevation patterns. The one row array was chosen primarily due to its wide elevation pattern coverage. This eliminates the need for elevation tracking, as the UAV is within the HPBW for all UAV ranges of interest. Adding a row of 8 more elements to increase the SNR will increase the cost of equipment. The additional SNR is not required, as the UAV transmitter power is sufficiently high. The sum and difference beams for the Matlab simulation, based on the derived pattern function of the one row array, are in agreement with the CST Microwave Studio simulations from the previous project by Gezer [2]. The printed circuit dipole element was found to have an E-plane pattern HPBW (80°) between that of an ideal dipole (90°) and a half-wave dipole (78°).

Several approaches for the demodulation of FM signals were explored. The considerations for the choice of the approaches for the FM demodulation are minimum circuitry, the ability to perform beamforming, recovery of the transmitted signal and the susceptibility to phase errors and LO drift. Three FM demodulation techniques are considered: Bilotti's quadrature demodulator, a local oscillator with no feedback and a digital phase locked loop quadrature detector. All three use digital beamforming and signal processing to demodulate the FM.

The Simulink models of the three FM demodulation techniques show satisfactory performance for the recovery of a two-tone signal. The simulations are done at a carrier frequency of 50 kHz, instead of 2.4 GHz, to greatly save on the simulation time. A LO

with no feedback is chosen, as it uses the least circuitry with satisfactory performance for the recovery of the two-tone signal. Beamforming can also be performed easily, as the raw I and Q data are preserved. This technique also eases the computer processing. Simulations were done with phase errors introduced in the channels and a frequency offset in the LO without feedback. The Simulink results indicate that the recovery of the two-tone signal can still be achieved with the expected LO drift.

Finally, the possible hardware components are briefly introduced in Chapter V. From the block diagram of the receiver module, the minimum power for the receiver module was used to determine the maximum operating range of the array using the one-way Friis equation.

B. RECOMMENDATIONS FOR FUTURE WORK

Simulations and studies should be conducted to analyze the following effects on the array and demodulation of FM signals.

1. Implementation of Signal Processing

The software necessary to do the beamforming and FM demodulation must be acquired or developed. The beamforming and tracking are relatively straightforward, and have been demonstrated by Gezer [2]. However, an acquisition method must be devised to acquire the signal when the antenna and processor are first turned on (or when the transmitter signal first appears). If the PLL method is used, the processor must compute the VCO error signal.

2. Hardware Tradeoff Studies

An appropriate ADC must be selected and interfaced with the AD8347 demodulator board, and controller software must be written. The hardware must be selected to minimize the amount of processing and control commands, so that real-time operation is possible.

APPENDIX A.   DIPOLES OF ARBITRARY ORIENTATION[4]

The dipole is centered at the origin as shown in Figure A1. The dipole direction is given by the vector:

$$\hat{I} = \hat{x}\underbrace{\sin\theta_a\cos\phi_a}_{u_a} + \hat{y}\underbrace{\sin\theta_a\sin\phi_a}_{v_a} + \hat{z}\underbrace{\cos\theta_a}_{w_a}$$

The dipole direction cosines are:

$$x \text{ direction cosine: } u_a = \cos\alpha_x = \sin\theta_a\cos\phi_a$$
$$y \text{ direction cosine: } v_a = \cos\alpha_y = \sin\theta_a\sin\phi_a$$
$$z \text{ direction cosine: } w_a = \cos\alpha_z = \cos\theta_a$$

The length of the dipole is L, and for a half-wave dipole the current distribution is given by the following function of the path length variable ℓ' :

$$I(\ell') = I_m\cos(k\ell'), \quad -L/2 \le \ell' \le L/2$$

where I_m is the maximum value at the feed point. For an ideal (Hertzian) dipole with constant current:

$$I(\ell') = I_m, \quad -L/2 \le \ell' \le L/2, \quad L << \lambda$$

The direction cosines for the far field observation point are:

$$x \text{ direction cosine: } u = \sin\theta\cos\phi$$
$$y \text{ direction cosine: } v = \sin\theta\sin\phi$$
$$z \text{ direction cosine: } w = \cos\theta$$

---

[4] The materials for Appendix A is from "Arbitary dipoles" unpublished notes of David C. Jenn.
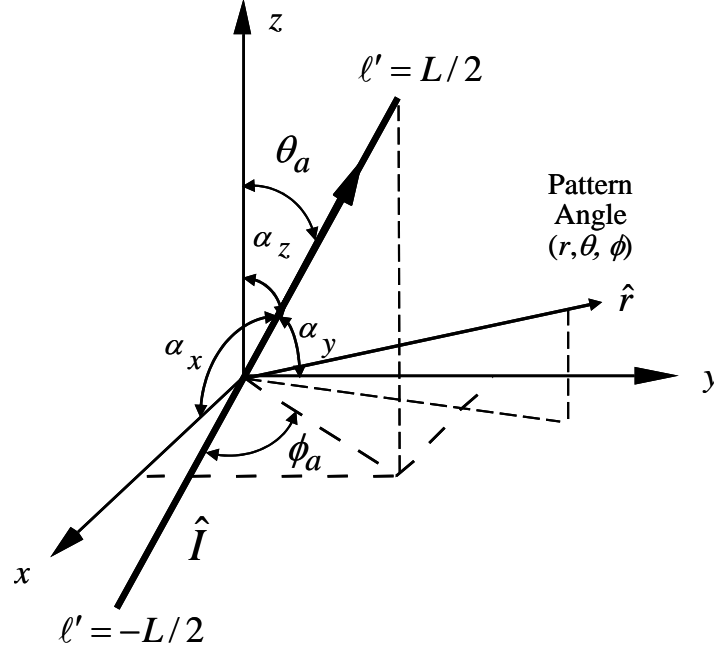
Figure A1: Dipole of arbitrary orientation centered at the origin

The far-field radiation integral can be written as:

$$\vec{E}(\theta,\phi) = \frac{-j\beta\eta_o\hat{I}}{4\pi r} e^{-j\beta r} \int_{-L/2}^{L/2} I(\ell')e^{j\beta\ell'(\hat{r}\bullet\hat{I})}d\ell'$$

where it is understood that the $\hat{r}$ component is discarded. For the ideal dipole the integral is:

$$\int_{-L/2}^{L/2} I(\ell')e^{j\beta\ell'(\hat{r}\bullet\hat{I})}d\ell' = I_m L \operatorname{sinc}\left(\frac{\beta L\,\hat{r}\bullet\hat{I}}{2}\right) \approx I_m L \quad (L << \lambda)$$

and the resulting spherical field components are:

$$E_\theta = \vec{E}(\theta,\phi)\bullet\hat{\theta} = \frac{-j\beta\eta_o I_m L}{4\pi r} e^{-j\beta r}\hat{I}\bullet\hat{\theta}$$

$$E_\phi = \vec{E}(\theta,\phi)\bullet\hat{\phi} = \frac{-j\beta\eta_o I_m L}{4\pi r} e^{-j\beta r}\hat{I}\bullet\hat{\phi}$$

From the transform tables:

$$\hat{\theta} = \hat{x}\cos\theta\cos\phi + \hat{y}\cos\theta\sin\phi - \hat{z}\sin\theta$$
$$\hat{\phi} = -\hat{x}\sin\phi + \hat{y}\cos\phi$$

For a Hertzian dipole along the z axis: $(\theta_a = \phi_a = 0°, \hat{I} = \hat{z})$

$$\hat{I}\bullet\hat{\theta} = \hat{z}\bullet\hat{\theta} = -\sin\theta$$
$$\hat{I}\bullet\hat{\phi} = \hat{z}\bullet\hat{\phi} = 0$$

and the fields reduce to the familiar results:

$$E_\theta = \frac{j\beta\eta_o I_m L}{4\pi r}e^{-j\beta r}\sin\theta$$
$$E_\phi = 0$$

For a half-wave dipole $(L = \lambda/2)$ the integral is:

$$\int_{-L/2}^{L/2} I_m\cos(\beta\ell')e^{j\beta\ell'(\hat{r}\bullet\hat{I})}d\ell' = \left\{\frac{I_m e^{j\beta\ell'(\hat{r}\bullet\hat{I})}\left[j\beta\ell'(\hat{r}\bullet\hat{I})\cos(\beta\ell') + \beta\sin(\beta\ell')\right]}{\left[\beta\ell'(\hat{r}\bullet\hat{I})\right]^2 + \beta^2}\right\}_{-L/2}^{L/2}$$

After applying some trigonometric identities, the final result for the far electric field is:

$$\vec{E}(\theta,\phi) = -\frac{j\eta_o I_m \hat{I}\ e^{-j\beta r}}{2\pi r}\frac{\cos\left(\frac{\pi}{2}\hat{r}\bullet\hat{I}\right)}{1-(\hat{r}\bullet\hat{I})^2}$$

For a half-wave dipole along the z axis: $\theta_a = \phi_a = 0°, \hat{I} = \hat{z}$
$$\hat{r}\bullet\hat{I} = \cos\theta = w$$
$$\hat{\theta}\bullet\hat{I} = -\sin\theta$$

$$E_\theta = \frac{j\eta_o I_m\ e^{-j\beta r}}{2\pi r}\left[\frac{\cos\left(\frac{\pi}{2}\cos\theta\right)}{\sin\theta}\right]$$
$$E_\phi = 0$$

For a half-wave dipole along the x axis: $\theta_a = 90°, \phi_a = 0°, \hat{I} = \hat{x}$

$$\hat{r} \bullet \hat{I} = \sin\theta\cos\phi = u$$
$$\hat{\theta} \bullet \hat{I} = \cos\theta\cos\phi$$
$$\hat{\phi} \bullet \hat{I} = -\sin\phi$$

$$E_\theta = \frac{j\eta_o I_m\, e^{-j\beta r}}{2\pi r} \left[\frac{\cos\left(\frac{\pi}{2}\sin\theta\cos\phi\right)}{1-\sin^2\theta\cos^2\phi} \right] \cos\theta\cos\phi$$

$$E_\phi = -\frac{j\eta_o I_m\, e^{-j\beta r}}{2\pi r} \left[\frac{\cos\left(\frac{\pi}{2}\sin\theta\cos\phi\right)}{1-\sin^2\theta\cos^2\phi} \right] \sin\phi$$

APPENDIX B.   MATLAB CODE FOR AN ARRAY OVER A GROUND PLANE

This Matlab code was used to compute the array pattern for 1 row and 2 row arrays and the sum and difference beams, using the formulas derived in Chapter II.

```
linear array of dipoles with a ground plane
% z is array axis; ground plane is the xz plane
% y is normal to ground plane
% option to select dipoles along x or z
% fixed to include Etheta and Ephi
% two dimensional array (scans in both x and z dimension)
% half-wave dipoles
clear
warning off
rad=pi/180;
f=2.4e9;
wave=3e8/f;
beta=2*pi/wave;
dz=0.065;
Nz=8; %no. of elements in a row
dx=0.1;
Nx=1; %To define the no. of rows
h=0.25*wave;
% select the dipole direction: 'x' or 'z'
dipdir='x';  % dipoles x directed (parallel case)
%dipdir='z';  % dipoles z directed (collinear case)
% select the dipole type: 'h'=halfwave, 's'=short (constant current)
diptype='s';
%diptype='h';
%phi=0 cut
% phi=0 vary theta (x-z plane)
phi=90*rad;
theta=[0:1:180]*rad; w=cos(theta);
thetas=90; phis=;%theta defines the yz plane; phi defines the xy plane;
% x is along the direction of the short dipole;
%y is perpendicular to the ground;
%z is perpendicular to the short dipole and parallel to the ground plane.
cts=cos(thetas*rad); u=sin(theta)*cos(phi); v=sin(theta)*sin(phi);
cps=cos(phis*rad);
alphaz=-beta*dz*cts;
alphax=-beta*dx*cps;
psiz=beta*dz*w+alphaz;
psix=beta*dx*u+alphax;
if dipdir=='z'  % colinear dipoles (z directed)
  if diptype=='s'
  EFtheta=2*sqrt(1-w.^2).*sin(beta*h*v);
  EFphi=0;
  end
  if diftype=='h'
  EFtheta=2*sqrt(1-w.^2).*sin(beta*h*v).*cos(pi*w/2)./sqrt(1-w.^2+1e-5);
```

73

```matlab
    EFphi=0;
    end
end
if dipdir=='x' % parallel case (x directed)
    if diptype=='s'
    EFtheta=2*cos(phi).*w.*sin(beta*h*v);
    EFphi=-2*sin(phi).*sin(beta*h*v);
    end
    if diptype=='h'
    EFtheta=2*cos(phi).*w.*sin(beta*h*v).*cos(pi*u/2)./(1-u.^2+1e-5);
    EFphi=-2*sin(phi).*sin(beta*h*v).*cos(pi*u/2);
    end
end
AF=sin(Nx*psix/2)./sin(psix/2).*sin(Nz*psiz/2)./sin(psiz/2);
caftheta=abs(AF.*EFtheta)/2/Nx/Nz;
cafphi=abs(AF.*EFphi)/2/Nx/Nz;
cafthdb=20*log10(caftheta+1e-5);
cafphdb=20*log10(cafphi+1e-5);
caf=sqrt(cafphi.^2+caftheta.^2);
cafdb=10*log10(caf.^2);
figure(1),clf
subplot(121)
polardb(theta/rad,cafthdb,'-')
title(['Polar dB plot E_\theta, \phi=',num2str(phi/rad),'^o'])
subplot(122)
polardb(theta/rad,cafphdb,'-')
title(['Polar dB plot E_\phi, \phi=',num2str(phi/rad),'^o'])
hold off
%theta=90 cut
clear theta phi AF caf cafthdb cafphdb EFth EFph psi u v w cts ct
% theta=90 vary theta (x-y plane)
phi=[0:1:180]*rad;
theta=89.99*rad; ct=cos(theta);
% note to always mantain the cut theta at 89.99 or 90.01
u=sin(theta)*cos(phi);
cts=cos(thetas*rad); v=sin(theta).*sin(phi); w=ones(1,length(v))*ct;
alphaz=-beta*dz*cts;
psiz=(beta*dz*cos(theta)+alphaz)*ones(length(phi),1)';
psix=(beta*dx*u+alphax);
if dipdir=='z'  % colinear dipoles (z directed)
    if diptype=='s'
    EFth=2*sqrt(1-w.^2).*sin(beta*h*v);
    EFph=0;
    end
    if diftype=='h'
    EFth=2*sqrt(1-w.^2).*sin(beta*h*v).*cos(pi*w/2)./sqrt(1-w.^2+1e-5);
    EFph=0;
    end
end
if dipdir=='x'  % parallel case (x directed)
    if diptype=='s'
    EFth=2*cos(phi).*w.*sin(beta*h*v);
    EFph=-2*sin(phi).*sin(beta*h*v);
    end
    if diptype=='h'
```

```
    EFth=2*cos(phi).*w.*sin(beta*h*v).*cos(pi*u/2)./(1-u.^2+1e-5);
    EFph=-2*sin(phi).*sin(beta*h*v).*cos(pi*u/2);
    end
end
AF=sin(Nx*psix/2)./sin(psix/2).*sin(Nz*psiz/2)./sin(psiz/2);
caftheta=abs(AF.*EFth)/2/Nx/Nz;
cafphi=abs(AF.*EFph)/2/Nx/Nz;
cafthdb=20*log10(caftheta+1e-5);
cafphdb=20*log10(cafphi+1e-5);
caf=sqrt(cafphi.^2+caftheta.^2);
cafdb=10*log10(caf.^2);
figure(2),clf
subplot(121)
polardb(phi/rad,cafthdb,'-')
title(['Polar dB plot E_\theta, \theta=',num2str(theta/rad),'^o'])
subplot(122)
polardb(phi/rad,cafphdb,'-')% plot for E phi figure 2
title(['Polar dB plot E_\phi, \theta=',num2str(theta/rad),'^o'])
hold off
% clear theta phi AF caf cafdb EFth EFph psi
% 3-D plot %
iplt3d=1; % skip 3d plots if =1
if iplt3d==0
 it=0;
 for th=0:3:180
   jt=0; it=it+1;
  for ph=0:3:360
    jt=jt+1;
    thr=th*rad;
    phr=ph*rad;
    phd(it,jt)=ph;
    thd(it,jt)=th;
    ct=cos(thr);
    st=sin(thr);
    u=sin(thr)*cos(phr);
    v=sin(thr)*sin(phr);
    w=cos(thr);
    xsiz=beta*dz*cos(thr)-alpha;
    xsix=beta*dx*u;
    E=0;
    if v>=0;  % upper half space (lower half space zero)
        E=sin(Nz*xsiz/2)/sin(xsiz/2)*sin(Nx*xsix/2)/sin(xsix/2);
        if E==NaN, E=Nx*Nz; end
    end
    if dipdir=='z'
       EFth=2*sqrt(1-w^2)*sin(beta*h*v); % colinear dipoles (z directed)
       EFph=0;
    end
    if dipdir=='x'
       EFth=2*cos(phr).*w*sin(beta*h*v);  % parallel case (x directed)
       EFph=-2*sin(phr)*sin(beta*h*v);
    end
    ffth=abs(EFth*E);
    ffph=abs(EFph*E);
    fth(it,jt)=ffth;
```

75

```matlab
            fph(it,jt)=ffph;
            Xth(it,jt)=fth(it,jt)*u;
            Yth(it,jt)=fth(it,jt)*v;
            Zth(it,jt)=fth(it,jt)*w;
            Xph(it,jt)=fph(it,jt)*u;
            Yph(it,jt)=fph(it,jt)*v;
            Zph(it,jt)=fph(it,jt)*w;
        end
     end
    %plot theta component
    MAX=max([max(max(Xth)),max(max(Yth)),max(max(Zth)),max(max(Xph)),max(max(Yph)),max(max(Zph))]);
    figure(3),clf
    mesh(Xth/MAX,Yth/MAX,Zth/MAX)
    axis([-1,1,-1,1,-1,1])
    axis square
    hold on
    % spread N elements along the z axis between [-1,1]
    z0=[-(Nz-1)/2:(Nz-1)/2]*.75/Nz;
    x0=[-(Nx-1)/2:(Nx-1)/2]*.25/Nx;
    [X,Z]=meshgrid(x0,z0); Y=ones(size(X))*.05;
    plot3(X,Y,Z,'ko')
    xlabel('X=|E|sin(t)cos(p)')
    ylabel('Y=|E|sin(t)sin(p)')
    zlabel('Z=|E|cos(t)');
    if dipdir=='x', title('E_\theta for x directed dipoles (parallel case)'), end
    if dipdir=='z', title('E_\theta for z directed dipoles (collinear case)'), end

    %plot phi component
    figure(4),clf
    mesh(Xph/MAX,Yph/MAX,Zph/MAX)
    axis([-1,1,-1,1,-1,1])
    axis square
    hold on
    % spread N elements along the z axis between [-1,1]
    z0=[-(Nz-1)/2:(Nz-1)/2]*.75/Nz;
    x0=[-(Nx-1)/2:(Nx-1)/2]*.25/Nx;
    [X,Z]=meshgrid(x0,z0); Y=ones(size(X))*.05;
    plot3(X,Y,Z,'ko')
    xlabel('X=|E|sin(t)cos(p)')
    ylabel('Y=|E|sin(t)sin(p)')
    zlabel('Z=|E|cos(t)');
    if dipdir=='x', title('E_\phi for x directed dipoles (parallel case)'), end
    if dipdir=='z', title('E_\phi for z directed dipoles (collinear case)'), end
    end
```

APPENDIX C.   MATLAB CODES FOR BILOTTI'S METHOD

This Matlab code was used to compute the voltage ratio versus frequency using the formulas derived in Chapter V.

```
% FM quadrature demod
% from note by Coffing and Main
clear
rad=pi/180;
L=.45e-9; Cp=5e-12; Cs=5e-12; Rp=560000;
cc=Cs/(Cs+Cp);
wn=1/sqrt(L*(Cs+Cp));
Q=Rp/wn/L;
fn=wn/2/pi;
disp(['Cs = ',num2str(Cs)])
disp(['Cp = ',num2str(Cp)])
disp(['L = ',num2str(L)])
disp(['fn = ',num2str(fn/1e6),' MHz'])
disp(['Q = ',num2str(Q)])
% frequencies in MHz
f1=2365;
f2=2380;
df=1;
nf=floor((f2-f1)/df)+1;
for i=1:nf
    fmhz(i)=f1+(i-1)*df;
    f=fmhz(i)*1e6;
    w=2*pi*f;  % omega
    s=j*w;
    ww=w/wn;
    wp=w+wn;
    wm=w-wn;
    H(i)=j*Q*cc*ww/(1+j*Q/ww*(wp*wm/wn^2));
    a=2*Q*wm/wn;
    H1(i)=Cs*L*s^2/((Cp+Cs)*L*s^2+L*s/Rp+1);    % equation (2)
end
Hm=abs(H);
Ha=angle(H)/rad;
H1m=abs(H1);
H1a=angle(H1)/rad;

figure(1)
subplot(121)
plot(fmhz,Hm)
xlabel('Frequency, MHz')
ylabel('|v_2/v_1|, dB')
grid
subplot(122)
plot(fmhz,Ha)
xlabel('Frequency, MHz')
ylabel('Angle v_2/v_1, Degrees')
grid
```

77

```
figure(2)
subplot(121)
plot(fmhz,H1m)
xlabel('Frequency, MHz')
ylabel('|v_2/v_1|, dB')
grid
subplot(122)
plot(fmhz,H1a)
xlabel('Frequency, MHz')
ylabel('Angle v_2/v_1, Degrees')
grid
```

LIST OF REFERENCES

[1]   Alan J. Fenn, Donald H. Temme, William P. Delaney, and William E. Courtney, "The Development of Phased-Array Radar Technology," http://www.ll.mit.edu/news/journal/pdf/vol12_no2/12_2devphasedarray.pdf, Volume 12, Number 2, 2000 Lincoln Laboratory Journal, last visited October 2007.

[2]   Berat Levent Gezer, "Multi-beam digital antenna for radar, communications and UAV tracking based on off-the-shelf wireless technologies," Master's Thesis, Naval Postgraduate School, Monterey, California, September 2006.

[3]   Dr. Alison Brown, Randy Silva; *NAVSYS Corporation*, "A GPS Digital Phased Array Antenna and Receiver," http://www.navsys.com/Papers/0005004.pdf, NAVSYS PROPRIETARY, last visited October 2007.

[4]   "Active Phased Array Radar (APAR)," Document No. 1544.006-17 Rev. 02 – 12 October 2005, http://www.thales-systems.ca/projects/apar/apar.pdf, Thales Canada, System Division, last visited October 2007.

[5]   Brittin C. Kane, Member, IEEE, Larry A. Geis, Member, IEEE,Michael A. Wyatt, Member, IEEE, David G. Copeland, Member, IEEE, and Jeffrey A. Mogensen, Member, IEEE, "Smart Phased Array SoCs: A Novel Application for Advanced SiGe HBT BiCMOS Technology," http://www.insytecorp.com/documents/Phased_Array_SoCs.pdf, Proceedings of the IEEE, Vol. 93, No. 9, September 2005, last visited October 2007.

[6]   "Passive Phased Arrays," http://www.emsdss.com/pdf/PassivePhasedArraysApNote.pdf, EMS Technologies, Inc. Space and Technology, December 2005, last visited October 2007.

[7]   John A. Bartee, "Genetic algorithms as a tool for phased array radar design," Master's Thesis, Naval Postgraduate School, Monterey, California, June 2002.

[8]   L. C. Esswein, "Generic algorithm design and testing of a random element 3-D 2.4 GHz phased array transmit antenna constructed of commercial RF microchips," Master's Thesis, Naval Postgraduate School, Monterey, California, June 2003.

[9]   Eng Choon Yeo, "Wirelessly networked opportunistic digital phased array: System analysis and development of a 2.4 GHz demonstrator," Master's Thesis, Naval Postgraduate School, Monterey, California, December 2006.

[10]   Lawrence C. Trost, "Unmanned Air Vehicles (UAVs) for Cooperative Monitoring,".http://www.cmc.sandia.gov/cmc-papers/sand2000-0185.pdf, Sandia National Laboratories, January 2000, last visited October 2007.

[11]   Pasi Suvikunnas, Pertti Vainikainen and Klaus Hugl, "The comparison methods of different geometric configurations of adaptive antenna arrays." http://publik.tuwien.ac.at/files/pub-et_4262.pdf, ," Institute of Digital Communications/ Radio Laboratory Helsinki University of Technology, 20th – 22nd February 2001, last visited October 2007.

[12]   David C. Jenn, "Digital Arrays," Naval Postgraduate School, California, 2007 (unpublished notes).

[13]   "ADI – Analog Dialogue/ Direct Digital Synthesis (DSS)," http://www.analog.com/library/analogdialogue/archives/38-08/dds.html, last visited October 2007.

[14]   Datasheet for AD8347 EVAL demodulator evaluation board, Analog Devices.

[15]   N. Levanon, *Radar Principles*, Wiley and Sons, 1988.

[16]   David C. Jenn, "Arrays with ground planes," Naval Postgraduate School, California, 2007 (unpublished notes)

[17]   "Antenna Basics - part 1," http://wireless.ictp.trieste.it/school_2003/lectures/struzak/Introduction_to_Digital _Radio/Antenna_Basics1, last visited October 2007.

[18]   Jean-Fu Kiang, "Chapter 1- Antennas," cc.ee.ntu.edu.tw/~jfkiang/electromagnetic%20wave/antenna.pdf, Department of Electrical Engineering and Graduate Institute of Communication Engineering National Taiwan University, last visited October 2007.

[19]   Dirk Heberling, " Basic Antennas," http://www.ihf.rwth-aachen.de/fileadmin/Internet/daten/lehre/Script2_0607.pdf, Courses Antenna Engineering, last visited October 2007

[20]   "Wikipedia The Free Encyclopedia –Amplitude-Comparison Monopulse," http://en.wikipedia.org/wiki/Amplitude_monopulse, last visited October 2007.

[21]   Merrill Skolnik, *Radar Handbook*, 2nd Edition, pp. 18.1-18.60, McGraw-Hill, New York, NY, 1990.

[22]   "2.4 GHz Wireless Video/Audio Transmission Links XL-2000/H, XL-2000/HP models," http://www.rf-links.com/pdf/xl-2000.pdf, last visited November 2007.

[23]   "ePanorama.net-Audio/Video Wiring Page,"
        http://links.epanorama.net/links/wire_av.html#wireless, last visited November
        2007.

[24]   G´eza KOLUMB´AN, Dept. of Electronic and Information Engineering,
        "Demodulation of FM Signals,"
        http://www.mit.bme.hu/research/chaos/kolumban/hk_public_html/eie331/
        handouts/pdf/tut331_05fm_dem.pdf, The Hong Kong Polytechnic University, last
        visited November 2007.

[25]   "Wikipedia The Free Encyclopedia –Phase-locked loop,"
        http://en.wikipedia.org/wiki/Phase-locked_loop, Last visited November 2007.

[26]   C.N. Wilson, "Featured Technology – Introducing Digital Techniques to Radio
        Products," http://www.wirelessdesignmag.com/pdfs/wdd060401_features2.
        pdf, last visited November 2007.

[27]   David K. Morgan, "CD4046B Phase-Locked Loop: A Versatile Building Block
        for Micropower Digital and Analog Applications,"
        http://focus.ti.com/lit/an/scha002a/scha002a.pdf, Texas Instruments, February
        2003, last visited November 2007.

[28]   " FM Detectors (Discriminators),"
        http://www.ycars.org/EFRA/Module%20B/fmdet.htm, last visited November
            2007.

[29]   " CommsDesign –A Quadrature Demodulator Tutorial,"
        http://www.commsdesign.com/showArticle.jhtml?articleID=192200456, last
        visited November 2007

[30]   " Digi-Key Catalog T073," http://dkc1.digikey.com/us/en/pdf/Current.html, last
        visited November 2007.

[31]   "Datasheet for Quadrature Demodulator AD8347," http://www.analog.com/
        UploadedFiles/Data_Sheets/230407246AD8347_a.pdf, last visited November
        2007.

[32]   " NI 9215 4-Channel, 100 kS/s, 16 bit, ± 10 V Simultaneors Sampling Analog
        Input Module," http://sine.ni.com/nips/cds/view/p/lang/en/nid/202555, last visited
        November 2007.

THIS PAGE INTENTIONALLY LEFT BLANK

INITIAL DISTRIBUTION LIST

1. Defense Technical Information Center
   Ft. Belvoir, Virginia

2. Dudley Knox Library
   Naval Postgraduate School
   Monterey, California

3. Chairman, Prof. Jeffrey B. Knorr
   Naval Postgraduate School
   Monterey, California

4. Prof. David C. Jenn
   Department of Electrical and Computer Engineering
   Monterey, California

5. Robert D. Broadston
   Department of Electrical and Computer Engineering
   Monterey, California

6. Hui Kok Meng, Edmund
   Singapore Technologies Marine Ltd.
   Singapore

7. David Netzer
   CDTEMS
   Monterey, California

8. Kevin Jones
   Department of Mechanical and Astronautical Engineering
   Montery, California